Supplementary Information (SI) for Journal of Materials Chemistry A.

Supporting Information

Phenothiazine-Based Self-Assembled Monolayers for Efficient Tin Perovskite Solar cells with Co-cations

Atika Abid,[‡] Arulmozhi Velusamy,[‡] Shakil N. Afraj, Waqas Pervez, Ting-Yu Su, Shao-Huan Hong, Cheng-Liang Liu, Ming-Chou Chen, and Eric Wei-Guang Diau**

Atika Abid, Prof. E. W.-G. Diau
Department of Applied Chemistry and Institute of Molecular Science, National Yang Ming Chiao Tung University, 1001 Ta-Hseuh Rd., Hsinchu 300093, Taiwan; Center for Emergent Functional Matter Science, National Yang Ming Chiao Tung University, 1001 Ta-Hseuh Rd., Hsinchu 300093, Taiwan.
E-mail: diau@nycu.edu.tw

Dr. A. Velusamy, S. N. Afraj, T.-Y. Su, Prof. M.-C. Chen
Department of Chemistry and Research Center of New Generation Light Driven Photovoltaic Modules
National Central University
Taoyuan 32001, Taiwan
Email: mcchen@ncu.edu.tw

Waqas Pervez,
Institute of Physics, University of Rostock, Albert-Einstein-Str. 23, 18059 Rostock, Germany.
E-mail: waqas.pervez@uni-rostock.de

S.-H. Hong, Prof. C.-L. Liu
Department of Materials Science and Engineering
National Taiwan University
Taipei 10617, Taiwan

[‡] Atika Abid. and A. Velusamy contributed equally to this work.

Experiments

Chemicals: FAI (Greatcell Solar), GAI (Greatcell Solar), MAI (Greatcell Solar), SnI_2 (99.999%, Alfa Aesar), SnF_2 (99%, Aldrich), DMSO (Aldrich), chlorobenzene (Aldrich), IPA (Aldrich), hexafluoro-2-propanol (HFP, TCI), $EDAI_2$ (Greatcell Solar) and self-assembled-monolayer (SAM) molecules. Distilled ethanol was prepared for soaking of ITO substrates into SAM solutions.

General characterization: ^1H, ^{13}C and ^{31}P NMR spectra were recorded using a Bruker 500 or a 300 instrument, with reference to solvent signals. Differential scanning calorimetry (DSC) was carried out on a Mettler DSC 822 instrument at a scan rate of 10 K/min. Thermogravimetric analysis (TGA) was performed on a Perkin Elmer TGA-7 thermal analysis system using dry nitrogen as a carrier gas at a flow rate of 40 mL/min. The UV–vis spectrum was characterized by a JASCO V-670 UV–vis spectrophotometer. Differential pulse voltammetry experiments were performed with a conventional three-electrode configuration (a platinum disk working electrode, an auxiliary platinum wire electrode, and a non-aqueous Ag reference electrode, with a supporting electrolyte of 0.1 M tetrabutylammonium hexafluorophosphate (dry $TBAPF_6$) in the specified dry solvent, using a CHI621C Electrochemical Analyzer (CH Instruments). Under N_2, the anhydrous organic material was dissolved in above 0.1 M *o*-dichlorobenzene solution to prepare a 10^{-3} M test solution. In each DPV experiment, 5 mL of the test solution is scanned together with Fc/Fc+ (also 10^{-3} M; as internal standard) under N_2. Electrochemical potentials were referenced to an Fc/Fc^+ internal standard (at +0.64 V). Mass spectrometric data were obtained with an JMS-700 HRMS instrument.

Device fabrication: Commercially available ITO glasses (1.9×1.9 cm2) were cleaned with IPA, acetone, and DI water through ultra-sonication method for 30 min, then kept into oven at

100 ºC for drying. The dried substrates were exposed to UV-ozone treatment for 30-minute then soaked in the ethanolic SAM solutions. The SAM solutions were prepared by thoroughly dissolving the SAM molecules (0.1 mM) in 20 mL of distilled ethanol. The soaked ITO substrates were left overnight to ensure uniform monolayer coverage. The ITO substrates were then thoroughly rinsed with ethanol to eliminate any unreacted SAM molecules, followed by drying on a hotplate at 100°C for 10 minutes. The substrates were again UV-ozone treated for 10 minutes, then moved to a nitrogen-filled glovebox to deposit the perovskite film. A 2-step sequential deposition of the perovskite layer, include the one containing SnI_2 (0.8 mM), SnF_2 (0.16 mM), $EDAI_2$ (0.008 mM) in DMSO and the other containing FAI in mixing with GaI and MaI in proportion of 75% and 25% in a cosolvent of IPA/HFP/CB (5:5:2, v/v/v, 1.2 mL). According to which a 40 μL of the SnI_2 solution was dropped on SAM coated ITO substrate at 6000 rpm for 1 minute. Then glove box was purged for ~10 min, and without annealing, 100 μL of FaI, FAI/GaI and FaI/MaI solution was dropped for ~40s onto the SnI_2-coated substrates and then subjected to spinning at 5000 rpm for 12 s. Then, the films were annealed at 70ºC for 10 minutes. Later, electron transport layer of C_{60} (thickness ~35 nm), a hole- blocking layer of BCP (thickness ~5 nm) and metal electrode of Ag (~100 nm) were deposited through thermal evaporation chamber at pressure ~5×10^{-6} Torr.

Characterization of films and devices: A field-emission scanning electron microscope (SEM, JEOL JSM-7800F PRIME) was employed to examine the surface and cross-sectional morphology of the thin films deposited on ITO substrates. An atomic-force microscope (AFM, VT SPM, SII Nanotechnology Lnc.), and Scanning Probe Microscopy (Bruker) was utilized to assess the roughness of the Bare ITO substrate, ITO covered with SAMs and the perovskite thin films. For all photophysical investigations, the perovskite films were encapsulated with glass substrate by using the optical adhesive (Norland 61, Thorlabs NOA61). The X-ray diffraction (XRD) patterns of the perovskite thin film samples were recorded using a Bruker D8-Advance diffractometer with Cu Kα radiation. The UV-visible spectrophotometer (V-780) with an integrating sphere (ISN-9011, JASCO) and a lab-built photoluminescence (PL) spectroscopy system were employed to study the photophysical properties. For the PL measurements, the perovskite samples were excited at 450 nm, and the emission spectra were recorded within the 700 to 1100 nm wavelength range.

The PL transients were recorded with a time-correlated single-photon counting (TCSPC) with the Fluotime 200, PicoQuant, system. When the samples were excited at 635 nm using a picosecond pulsed-diode laser (LDH-635, PicoQuant). The repetition rate of the laser used for all experiments was 25 MHz. *J-V* characteristic curves were measured by using the Keithley 2400 with a solar simulator (XES-40S1, SAN-EI), under standard one sun illumination conditions (AM 1.5G, 100 mW cm^{-2}). Before measurements, it was calibrated with standard Si referencecell (Oriel, PN 91150V, VLSI standard). A metal mask placed atop the device had area0.0225 cm^2. The incident photon-to-current conversion efficiency (IPCE) was assessed with a setup that included a Xe lamp (150 W, A-1010, PTi) and a monochromator (PTi). Calibration of the IPCE spectra was performed using a standard Si photodiode (S1337-1012BQ, Hamamatsu) before the measurements. XPS and ultraviolet photoelectron spectra (UPS) were performed (Thermo K-ALPHA Surface Analysis). UPS experiments were calibrated with the Fermi edge of gold surface and performed in a high vacuum (~10^{-9}Torr).

Electrochemical impedance spectroscopy (EIS) was conducted in the dark with an AC amplitude of 20 mV over a frequency range from 4 MHz to 1 Hz. A bias DC voltage (0.5 V) was applied.

Materials:

Starting materials (from Sigma Aldrich, Alfa, or TCI Chemical Co.) were reagent grade and were used without further purification unless otherwise indicated. Reaction solvents (DMF, and dioxane) were dried and distilled from CaH_2.

General Procedures for Final Target Compounds (1–3): Under a nitrogen atmosphere, the intermediate phosphonate ester (**5**, **7** or **9**) (1 eq.) was dissolved in anhydrous 1,4-dioxane (20 mL) at room temperature. Bromotrimethylsilane (10 eq.) was then added dropwise to the reaction mixture, which was stirred for 24 hours at room temperature. The solvent was removed using a rotary evaporator to yield a solid. The solid residue was dissolved in methanol (20 mL) at room temperature, and deionized water was added dropwise until the mixture became opaque. The solution was stirred for an additional 12 hours. The crude product was filtered and washed with deionized water. The final products were obtained as a white to light blue solid (yield = 90%).

Synthesis of **PTz²** (**1**): ^{1}H NMR (500 MHz, DMSO-d_6): δ (ppm) 7.21 (t, J = 7.5 Hz, 2H), 7.15 (d, J = 7.5 Hz, 2H), 6.99 (d, J = 8 Hz, 2H), 6.96 (t, J = 7.5 Hz, 2H), 4.05-4.00 (m, 2H), 2.06-1.99 (m, 2H). ^{13}C NMR (125 MHz, DMSO-d_6): δ (ppm) 144.42, 128.17, 127.55, 123.44, 123.10, 115.67, 42.32, 26.95, 25.91. ^{31}P NMR (202 MHz, DMSO-d_6): δ (ppm) 22.20. HRMS (HR-FAB [M]$^+$) calcd. for $C_{14}H_{14}NO_3PS$: 307.0432, Found: 307.1.

Synthesis of **PTz** (**2**): ^{1}H NMR (500 MHz, DMSO-d_6): δ (ppm) 7.20 (t, J = 8 Hz, 2H), 7.15 (d, J = 7.5 Hz, 2H), 7.04 (d, J = 8 Hz, 2H), 6.94 (t, J = 7.5 Hz, 2H), 3.86 (t, J = 7.5 Hz, 2H), 1.77-1.75 (m, 2H), 1.58-1.49 (m, 4H). ^{13}C NMR (125 MHz, DMSO-d_6): δ (ppm) 145.24, 128.06, 127.56, 124.02, 122.89, 116.24, 46.69, 28.17, 27.75, 27.63, 27.09, 20.79. ^{31}P NMR (202 MHz, DMSO-d_6): δ (ppm) 26.38. HRMS (HR-FAB [M]$^+$) calcd. for $C_{16}H_{18}NO_3PS$: 335.0745, Found: 335.1.

Synthesis of **PTzBr** (**3**): ^{1}H NMR (500 MHz, DMSO-d_6): δ (ppm) 7.35 (m, 4H), 6.98 (d, J = 9 Hz, 2H), 3.81 (t, J = 7 Hz, 2H), 1.71 (m, 2H), 1.56-1.47 (m, 4H). ^{13}C NMR (125 MHz, DMSO-d_6): δ (ppm) 144.26, 130.84, 129.51, 125.88, 118.09, 114.49, 46.91, 28.09, 27.42, 27.30, 26.98, 20.64. ^{31}P NMR (202 MHz, DMSO-d_6): δ (ppm) 25.91. HRMS (HR-FAB [M]$^+$) calcd. for $C_{16}H_{16}Br_2NO_3PS$: 490.8955, Found: 490.9.

Synthesis of 10-(2-bromoethyl)-10*H*-phenothiazine (4): Under anhydrous conditions, sodium hydride (2 eq.) was added to dimethylformamide (10 mL). 10*H*-phenothiazine (1 eq.) was then slowly transferred to the reaction mixture at 0 °C using dimethylformamide (10 mL) as the solvent. The mixture was stirred for 1 hour in an ice bath. Next, 1,2-dibromoethane (4 eq.) was added slowly to the resulting solution, and the reaction was heated to 90 °C for 12 hours. The reaction mixture was cooled to room temperature, and water was added slowly at 0 °C. The crude mixture was then extracted with ethyl acetate and washed with deionized water. The organic layer was dried over Na_2SO_4, concentrated and purified by column chromatography using ethylacetate/hexane as the eluent to obtain compound **4** as a colorless oil. ^{1}H NMR (500 MHz, $CDCl_3$): δ (ppm) 7.18-7.13 (m, 4H), 6.96-6.93 (m, 2H), 6.86 (d, J = 8 Hz, 2H), 4.27 (t, J = 7.6 Hz, 2H), 3.62 (t, J = 7.6 Hz, 2H).

Synthesis of diethyl (2-(10*H*-phenothiazin-10-yl)ethyl)phosphonate (5): Compound **4** (1 eq.) was dissolved in triethyl phosphite (20 eq.) under a nitrogen atmosphere, and the reaction mixture was heated to 165 °C for 18 hours. After cooling to room temperature, the solvent was removed under vacuum to afford the product as a light-yellow oil. ^{1}H NMR (500 MHz, $CDCl_3$): δ (ppm) 7.18-7.14 (m, 4H), 6.93 (t, J = 7.3 Hz, 2H), 6.89 (d, J = 8 Hz, 2H), 4.17-4.10 (m, 6H), 2.33-2.26 (m, 2H), 1.34 (t, J = 7 Hz, 6H). ^{31}P NMR (202 MHz, $CDCl_3$): δ (ppm) 28.70.

Synthesis of 10-(4-bromobutyl)-10*H*-phenothiazine (6): Compound **6** was synthesized in the same way as compound **4** using 1,4-dibromobutane. ^{1}H NMR (500 MHz, $CDCl_3$): δ (ppm) 7.17-7.13 (m, 4H), 6.92 (t, J = 7.5 Hz, 2H), 6.86 (d, J = 8.5 Hz, 2H), 3.91 (t, J = 6 Hz, 2H), 3.39 (t, J = 6 Hz, 2H), 1.98-1.96 (m, 4H).

Synthesis of diethyl (4-(10*H*-phenothiazin-10-yl)butyl)phosphonate (7): Compound **7** was synthesized in the same way as compound **5**. ^{1}H NMR (500 MHz, $CDCl_3$): δ (ppm) 7.16-7.13 (m, 4H), 6.91 (t, J = 7.5 Hz, 2H), 6.85 (d, J = 8 Hz, 2H), 4.06-4.02 (m, 4H), 3.88 (t, J = 7 Hz, 2H), 1.91-1.88 (m, 2H), 1.74-1.72 (m, 4H), 1.28 (t, J = 7.3 Hz, 6H). ^{31}P NMR (202 MHz, $CDCl_3$): δ (ppm) 31.75.

Synthesis of 3,7-dibromo-10-(4-bromobutyl)-10*H*-phenothiazine (8): The 10-(4-bromobutyl)-10*H*-phenothiazine (1 eq.) was added to the glacial acetic acid (10 mL). Then, bromine (2.5 eq.) was diluted in glacial acetic acid (2 mL) and added dropwise to the reaction mixture. The resulting reaction mixture was stirred for 16 hours at room temperature. The reaction was then quenched by adding a saturated aqueous solution of sodium thiosulphate. The mixture was extracted with ethyl acetate and deionized water, and the organic layer was dried over Na_2SO_4. The solvent was removed *in vacuo* to afford the crude product. The crude product was further purified by column chromatography using ethyl acetate/hexanes as the eluent, to give compound **8** as a yellow liquid. ^{1}H NMR (500 MHz, $CDCl_3$): δ (ppm) 7.26-7.24 (m, 4H), 6.70 (d, J = 8.5 Hz, 2H), 3.82 (m, 2H), 3.38 (t, J = 6 Hz, 2H), 1.96-1.93 (m, 4H).

Synthesis of diethyl (4-(3,7-dibromo-10*H*-phenothiazin-10-yl)butyl)phosphonate (9): Compound **9** was synthesized in the same way as compound **5**. ^{1}H NMR (500 MHz, $CDCl_3$): δ (ppm) 7.28-7.26 (m, 4H), 6.71 (d, J = 8.5 Hz, 2H), 4.08-4.03 (m, 4H), 3.82 (t, J = 7 Hz, 2H), 1.89-1.86 (m, 2H), 1.74-1.73 (m, 4H), 1.30 (t, J = 7 Hz, 6H). ^{31}P NMR (202 MHz, $CDCl_3$): δ (ppm) 31.51.

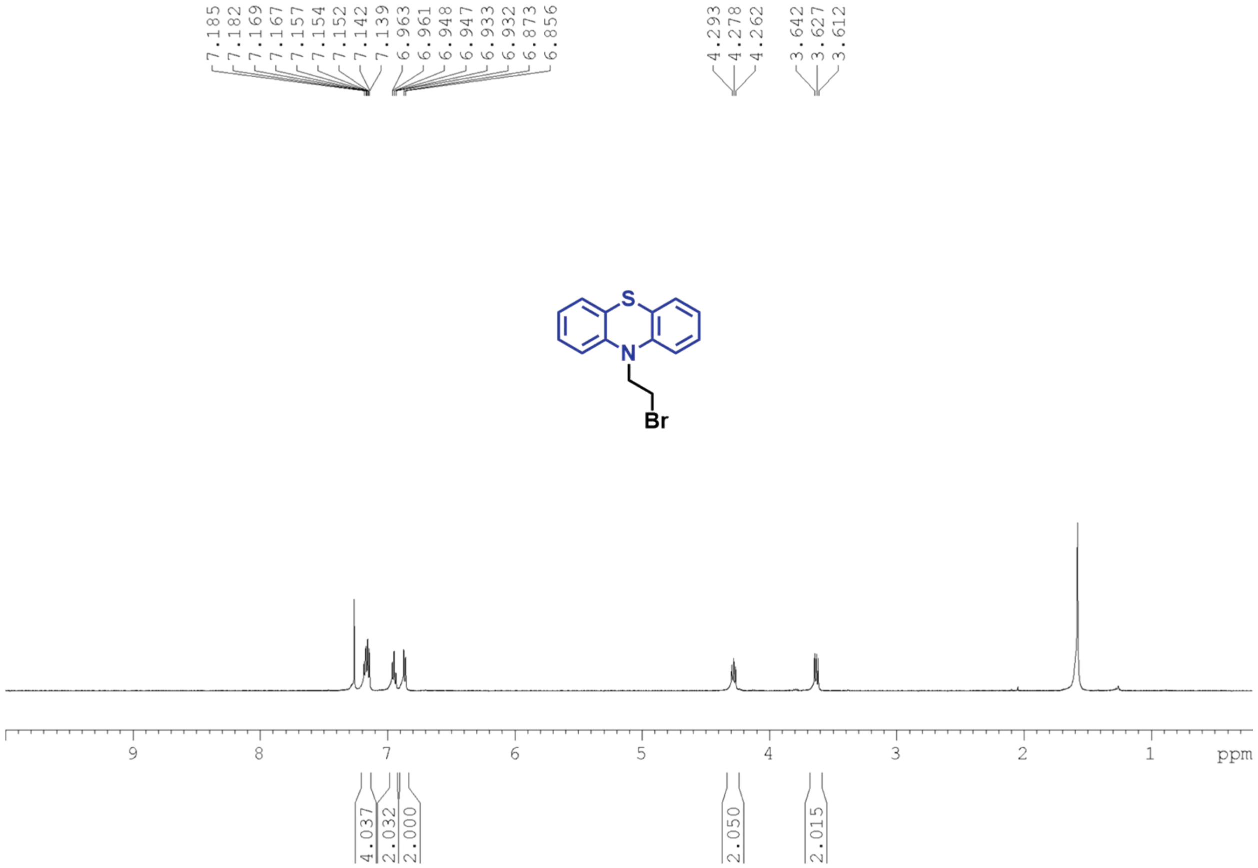

Figure S1. ^{1}H NMR spectrum of compound **4** in CDCl$_3$.

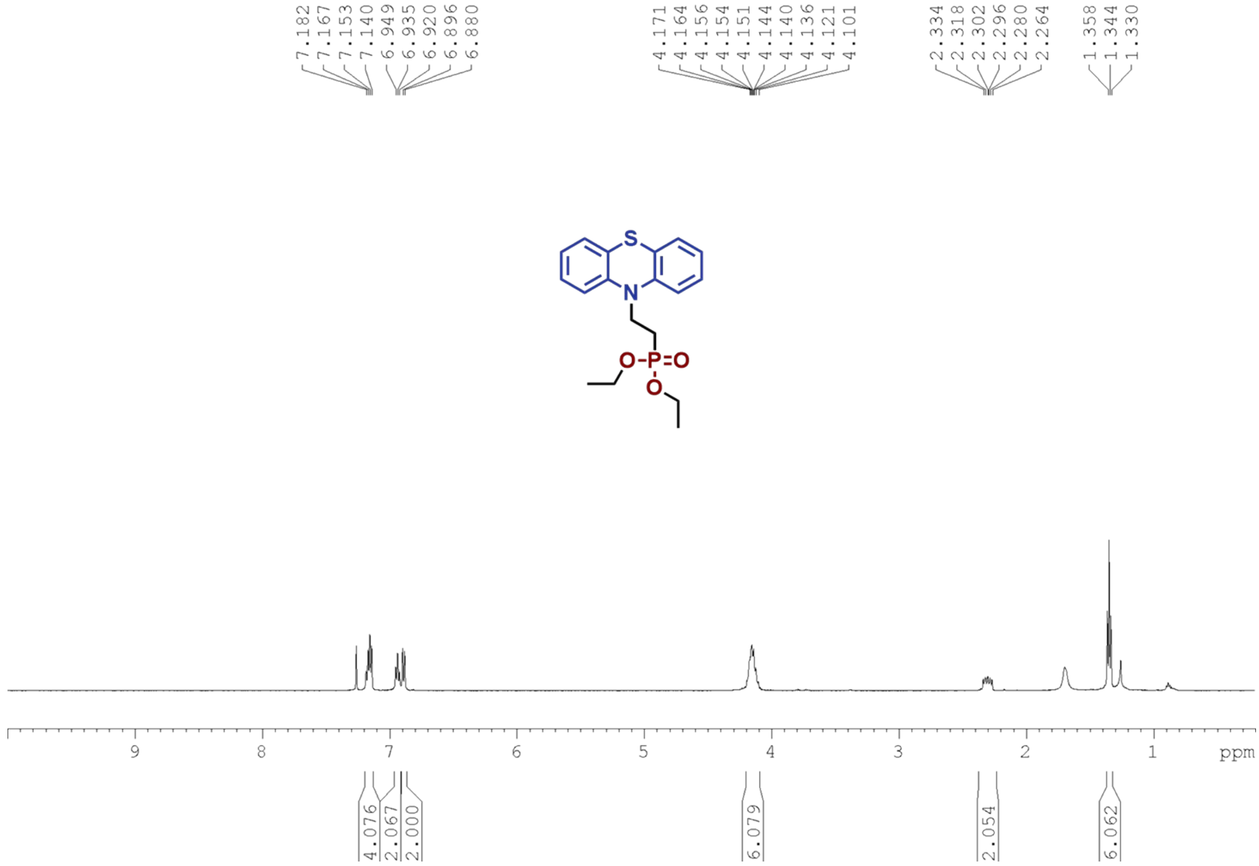

Figure S2. ^{1}H NMR spectrum of compound **5** in CDCl$_3$.

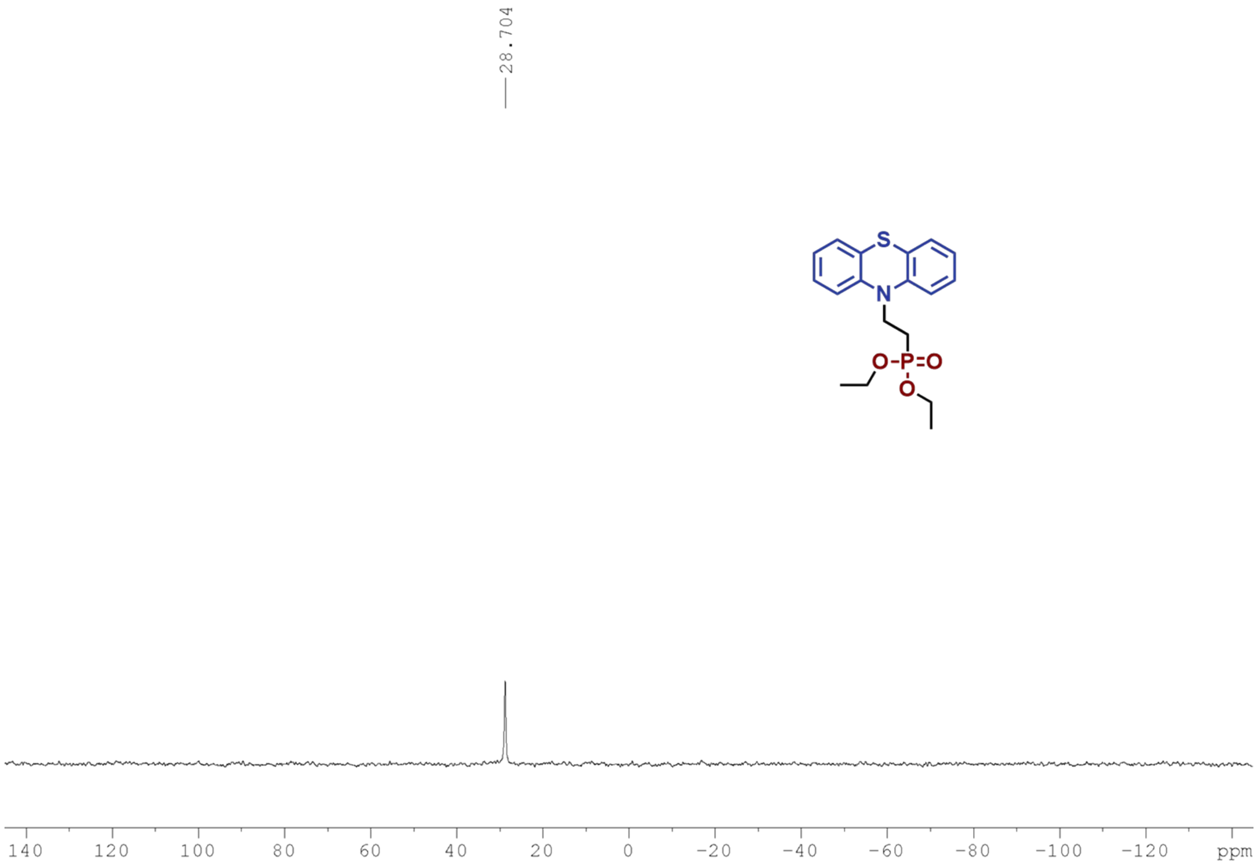

Figure S3. ^{31}P NMR spectrum of compound **5** in $CDCl_3$.

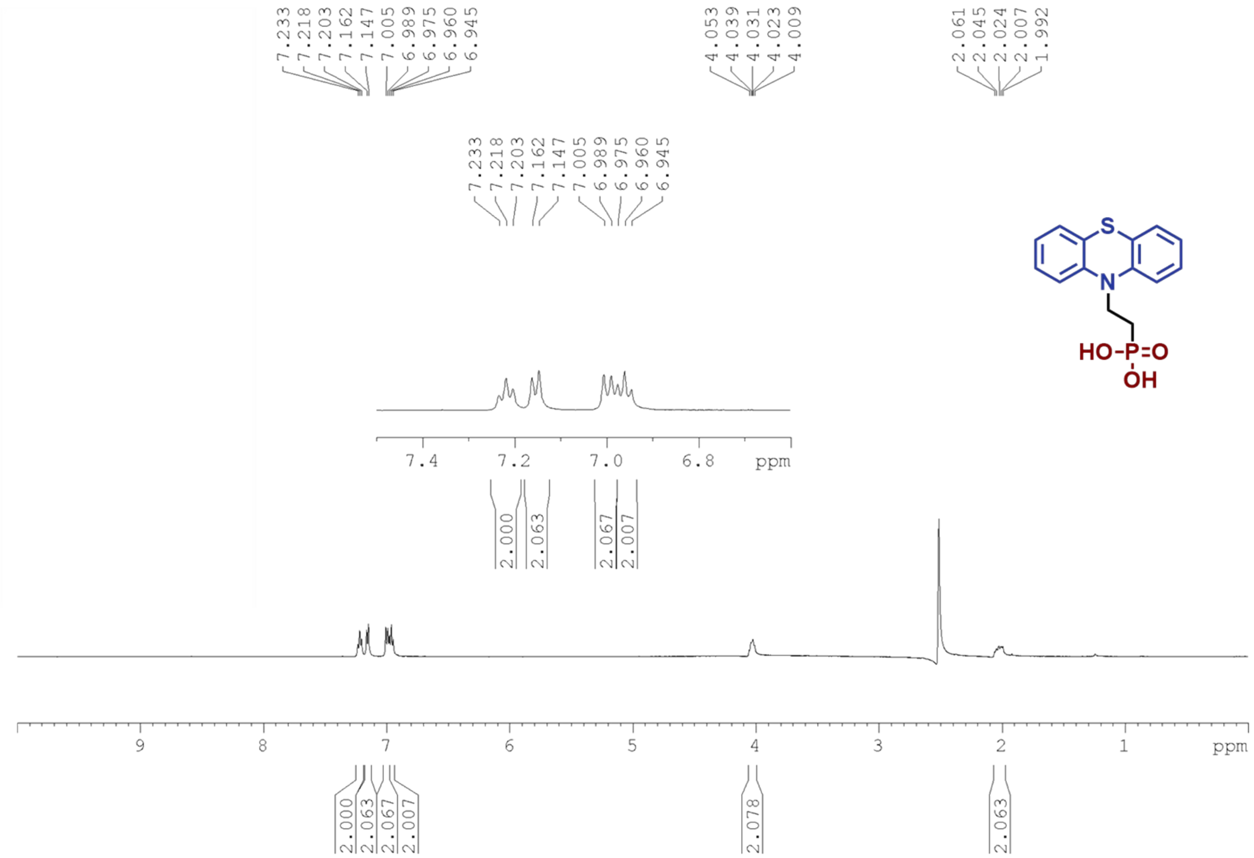

Figure S4. ^{1}H NMR spectrum of **PTz^2** (**1**) in DMSO-d_6.

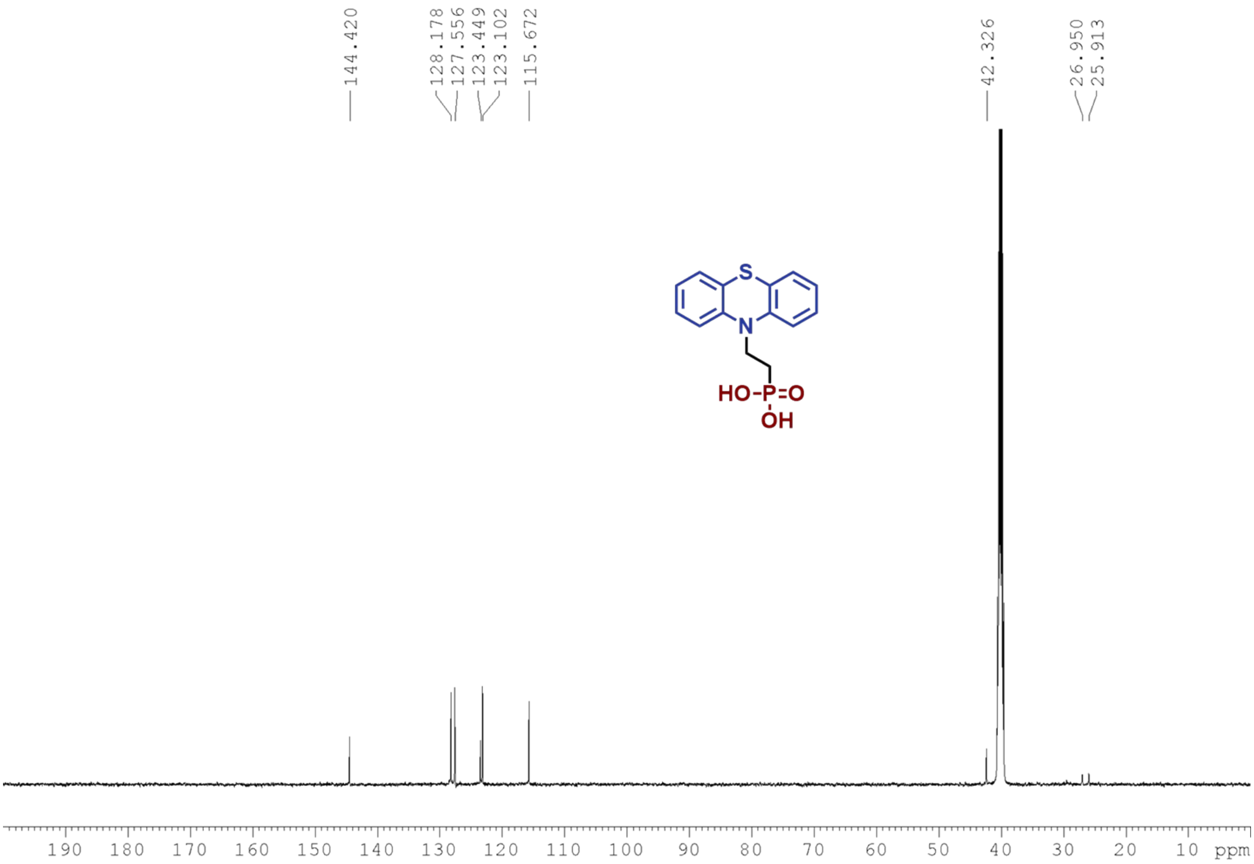

Figure S5. ^{13}C NMR spectrum of **PTz²** (**1**) in DMSO-d_6.

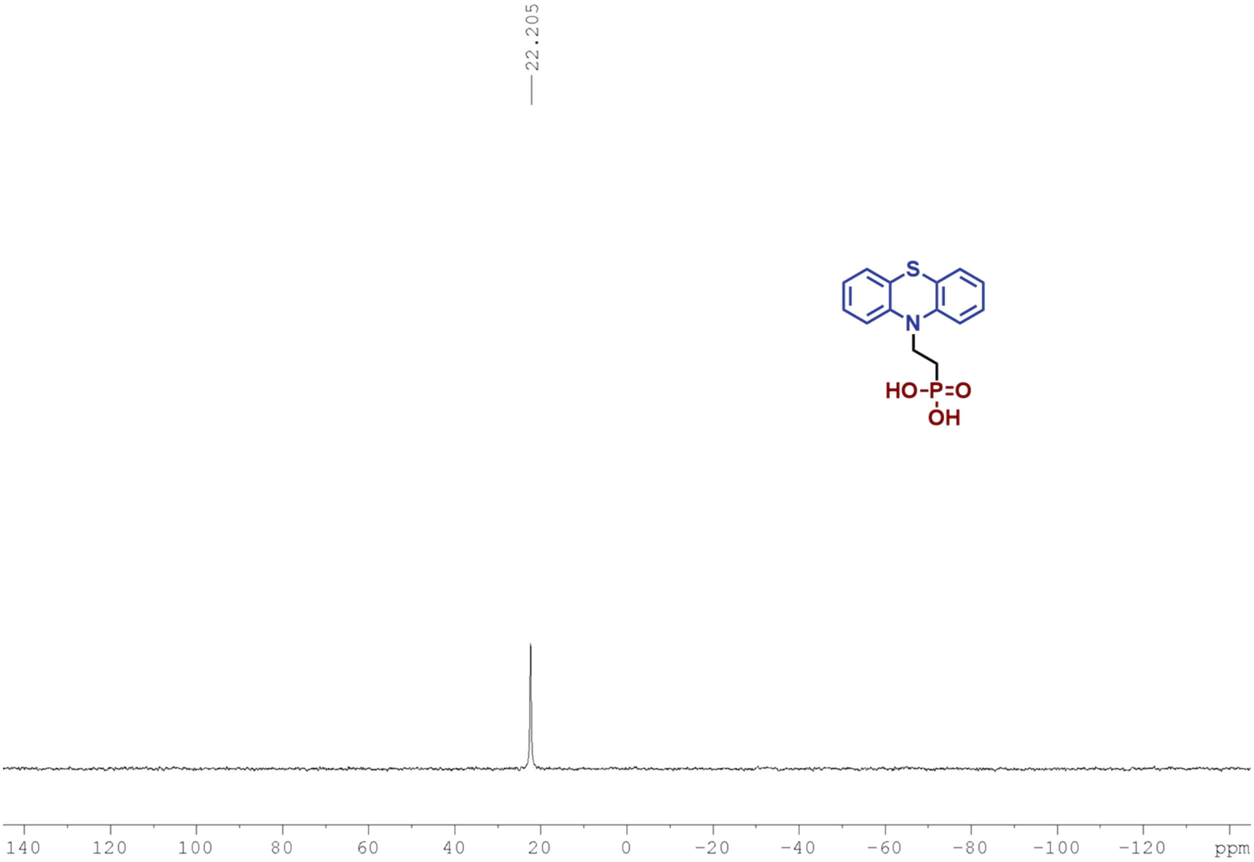

Figure S6. ^{31}P NMR spectrum of **PTz²** (**1**) in DMSO-d_6.

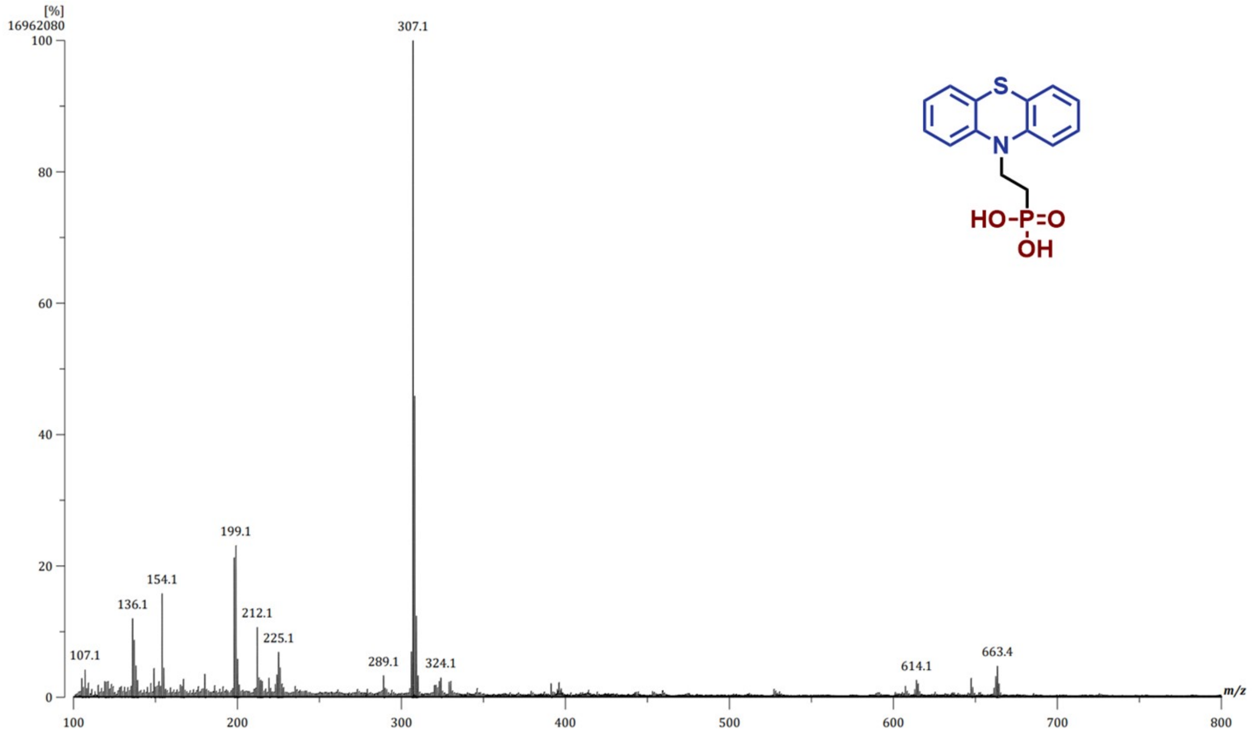

Figure S7. HRMS spectrum of **PTz^2** (**1**).

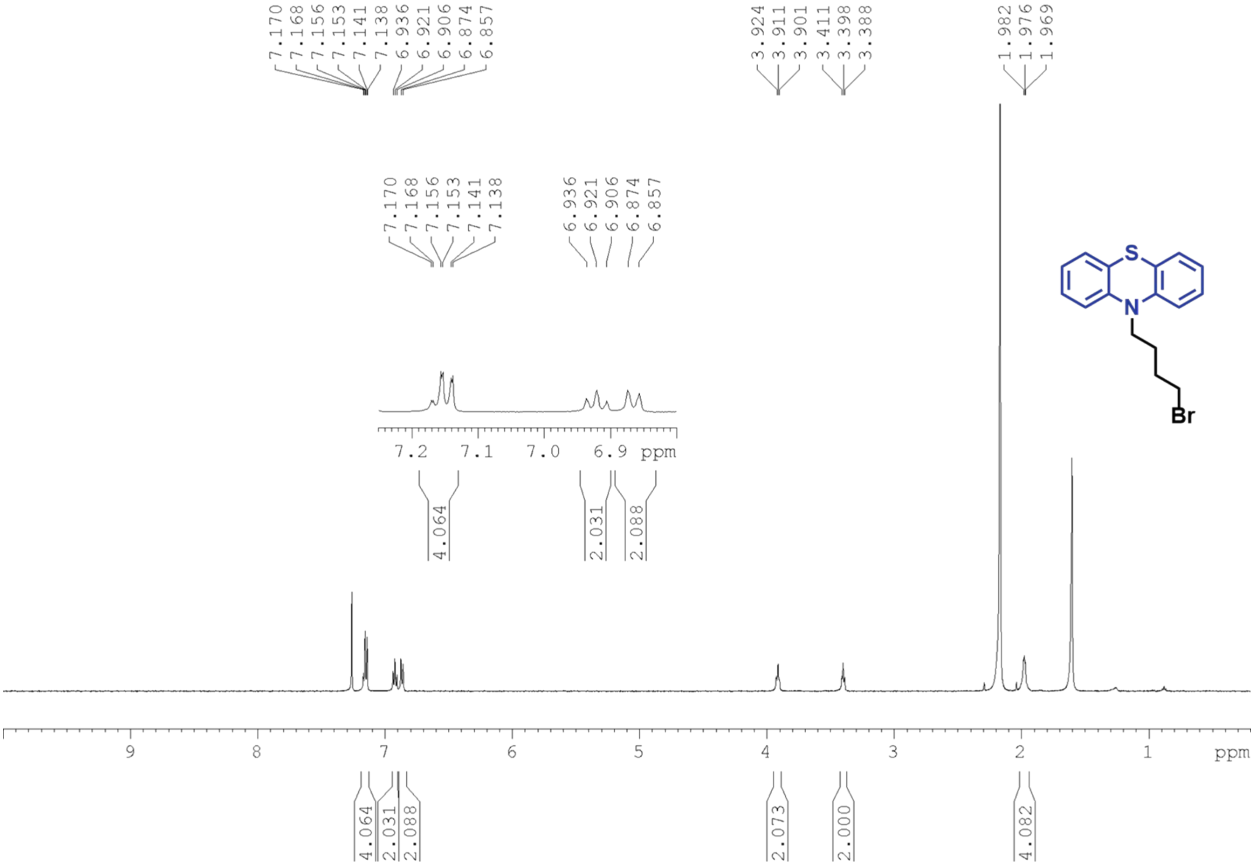

Figure S8. ^{1}H NMR spectrum of compound **6** in $CDCl_3$.

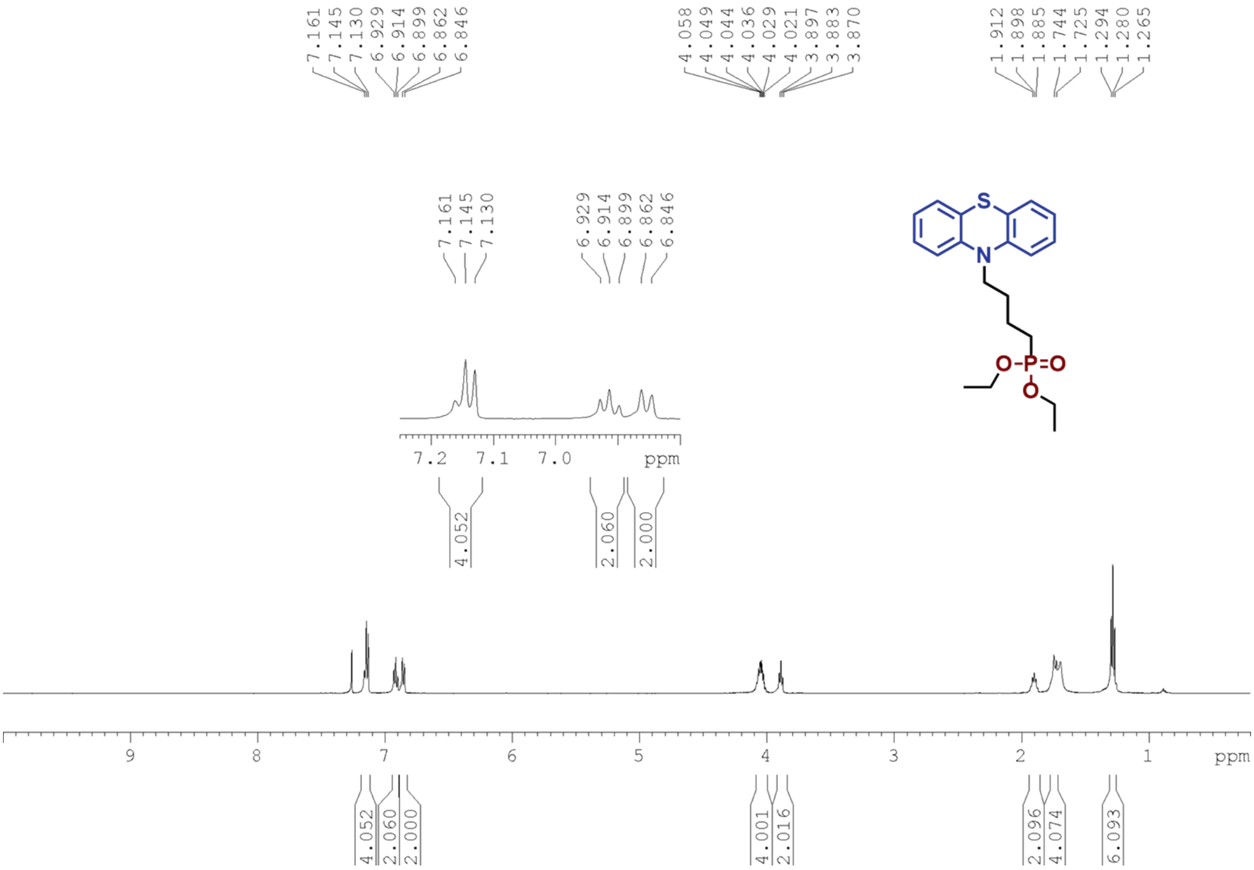

Figure S9. ^{1}H NMR spectrum of compound **7** in $CDCl_3$.

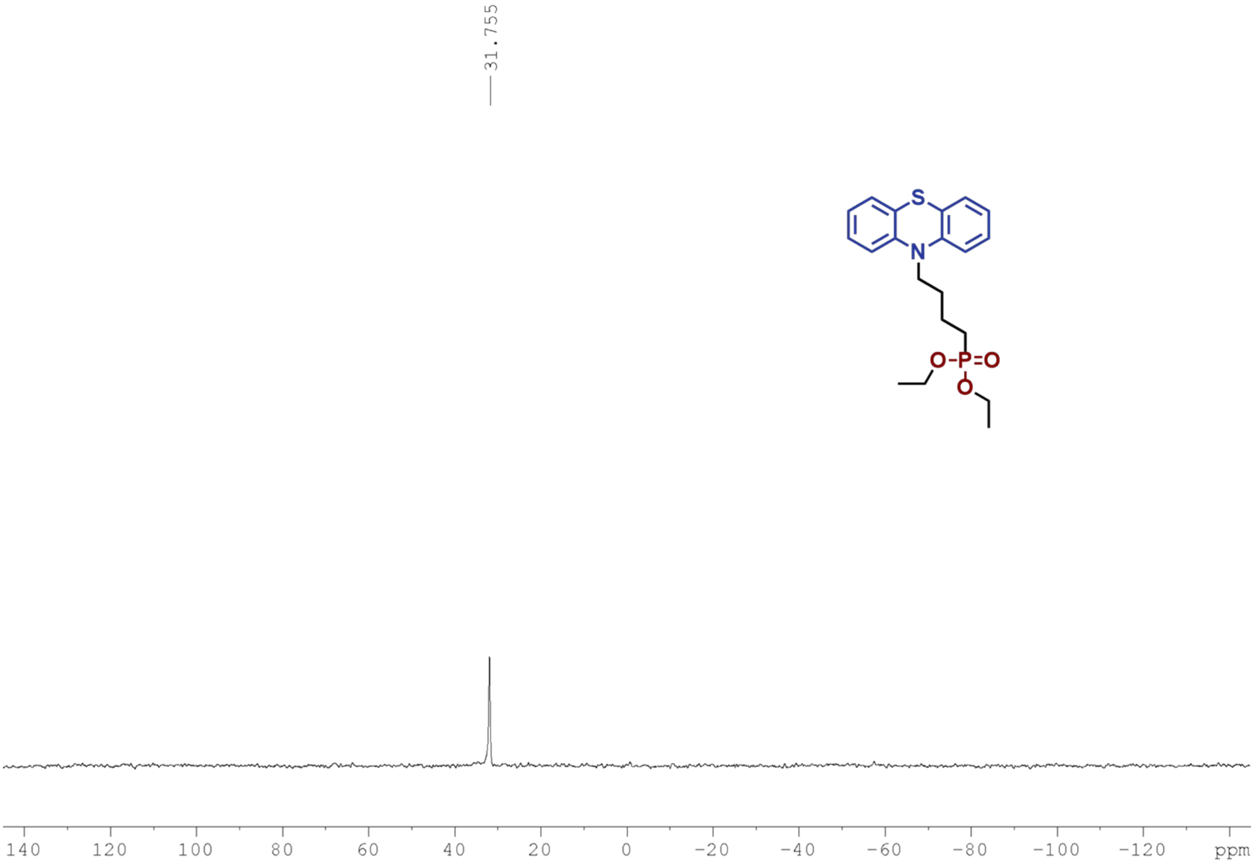

Figure S10. ^{31}P NMR spectrum of compound **7** in $CDCl_3$.

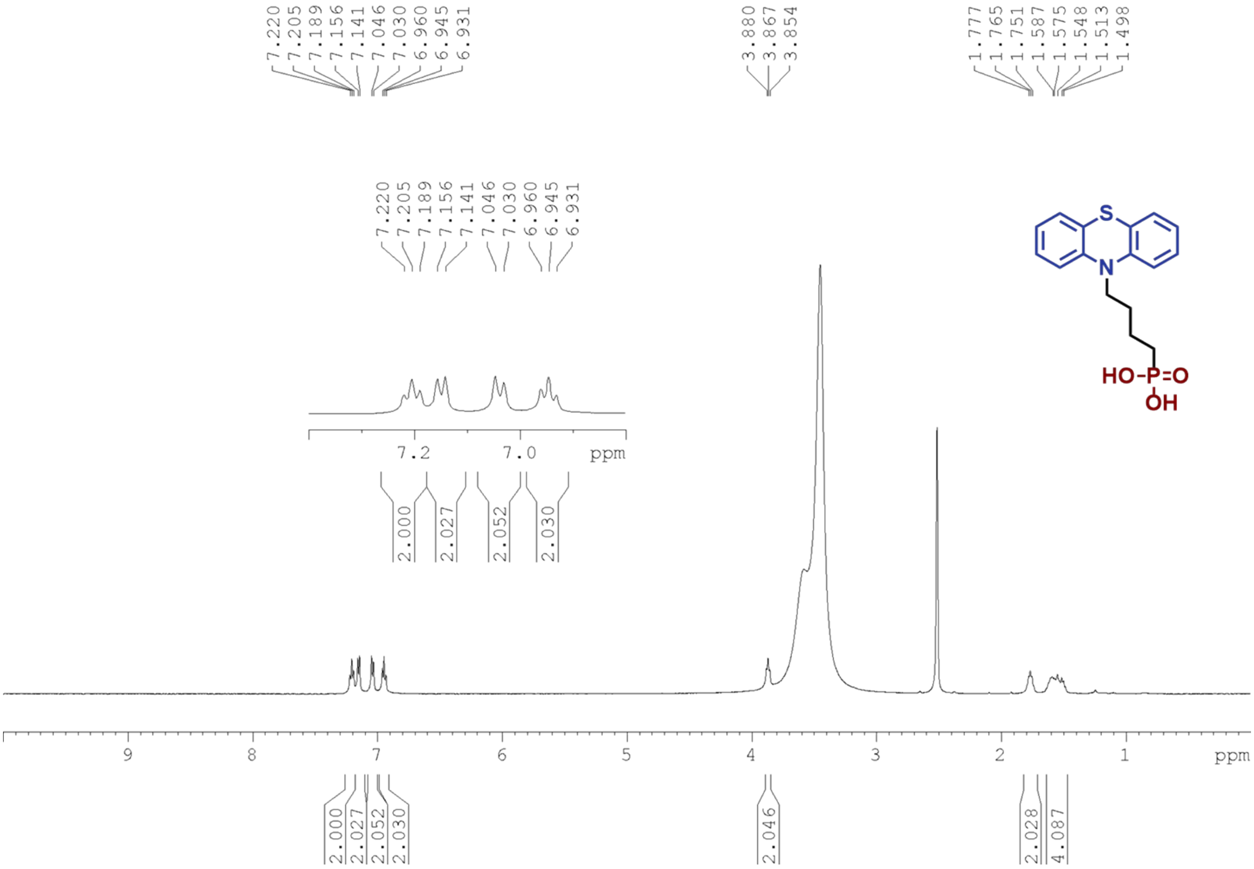

Figure S11. ^{1}H NMR spectrum of **PTz** (**2**) in DMSO-d_6.

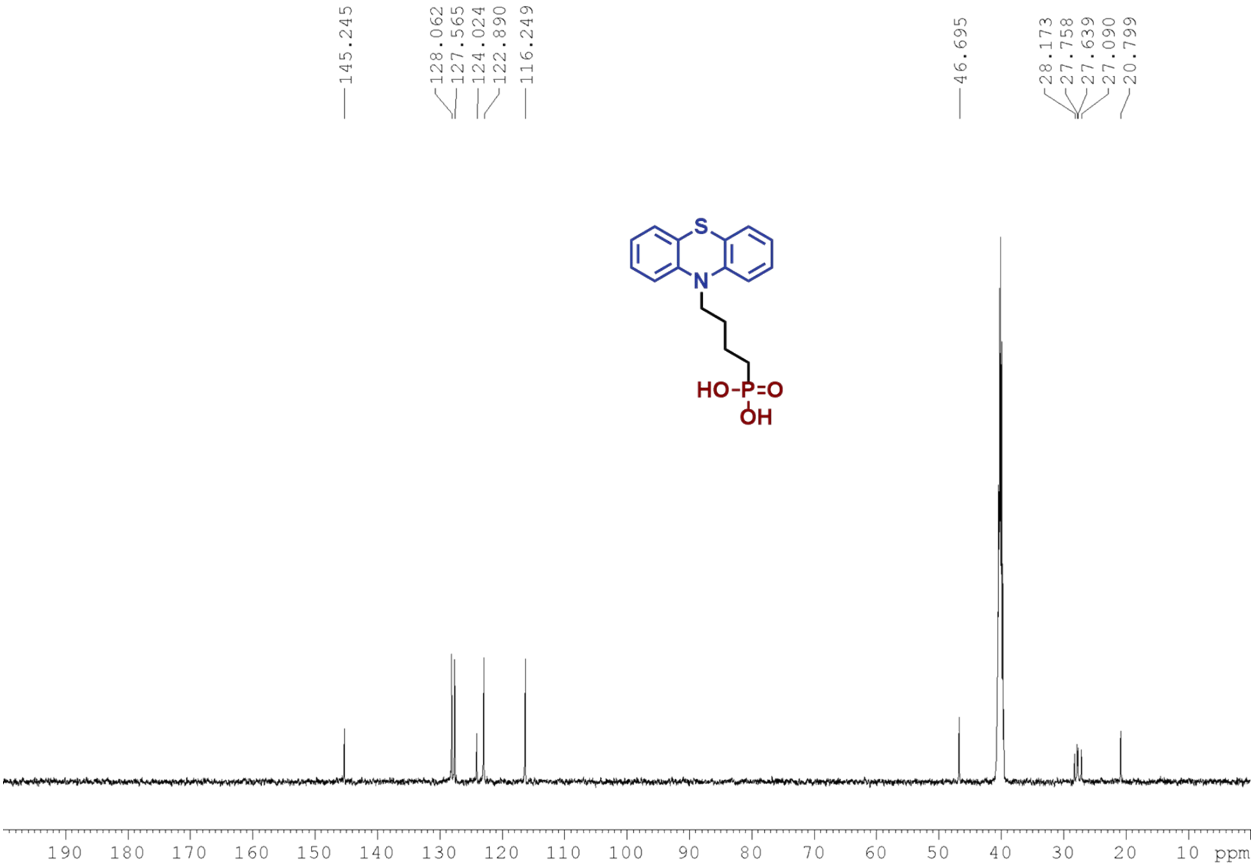

Figure S12. ^{13}C NMR spectrum of **PTz** (**2**) in DMSO-d_6.

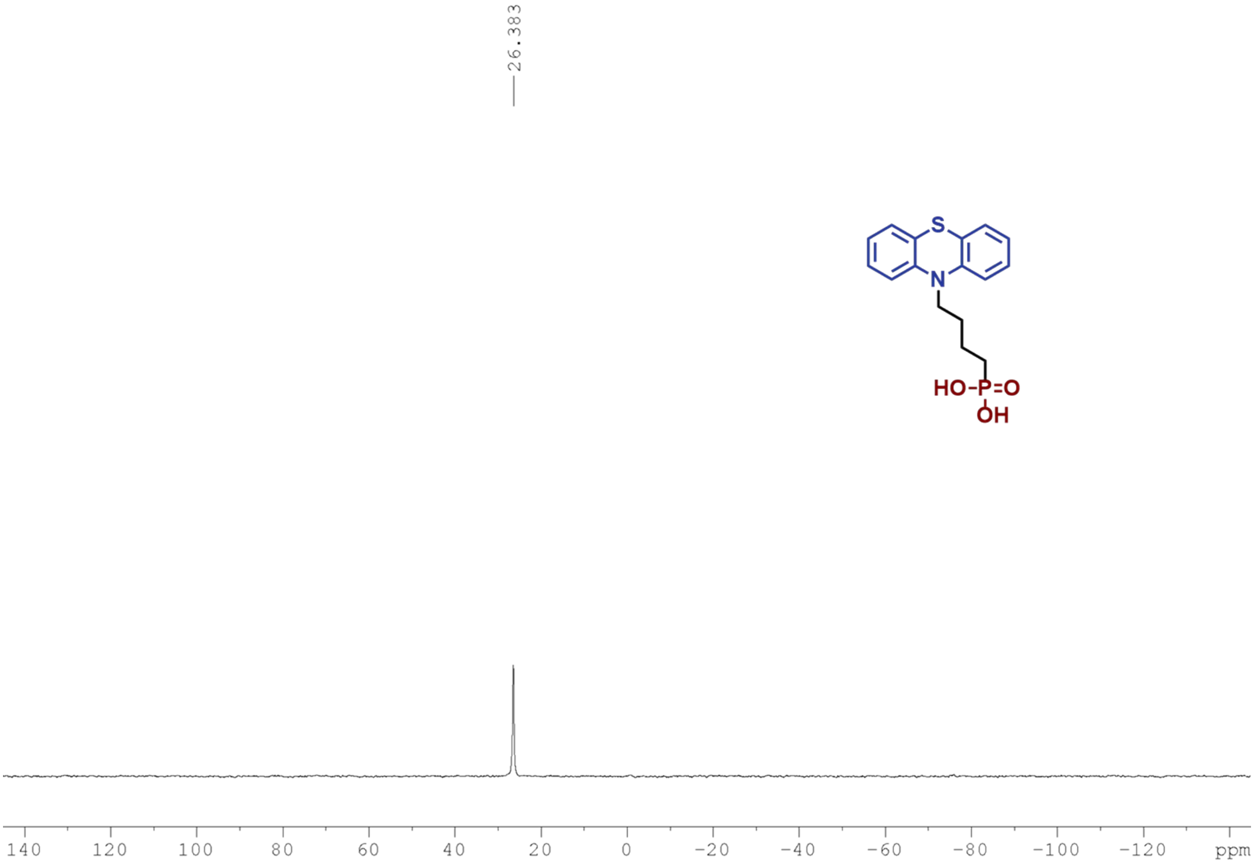

Figure S13. ^{31}P NMR spectrum of **PTz** (**2**) in DMSO-d_6.

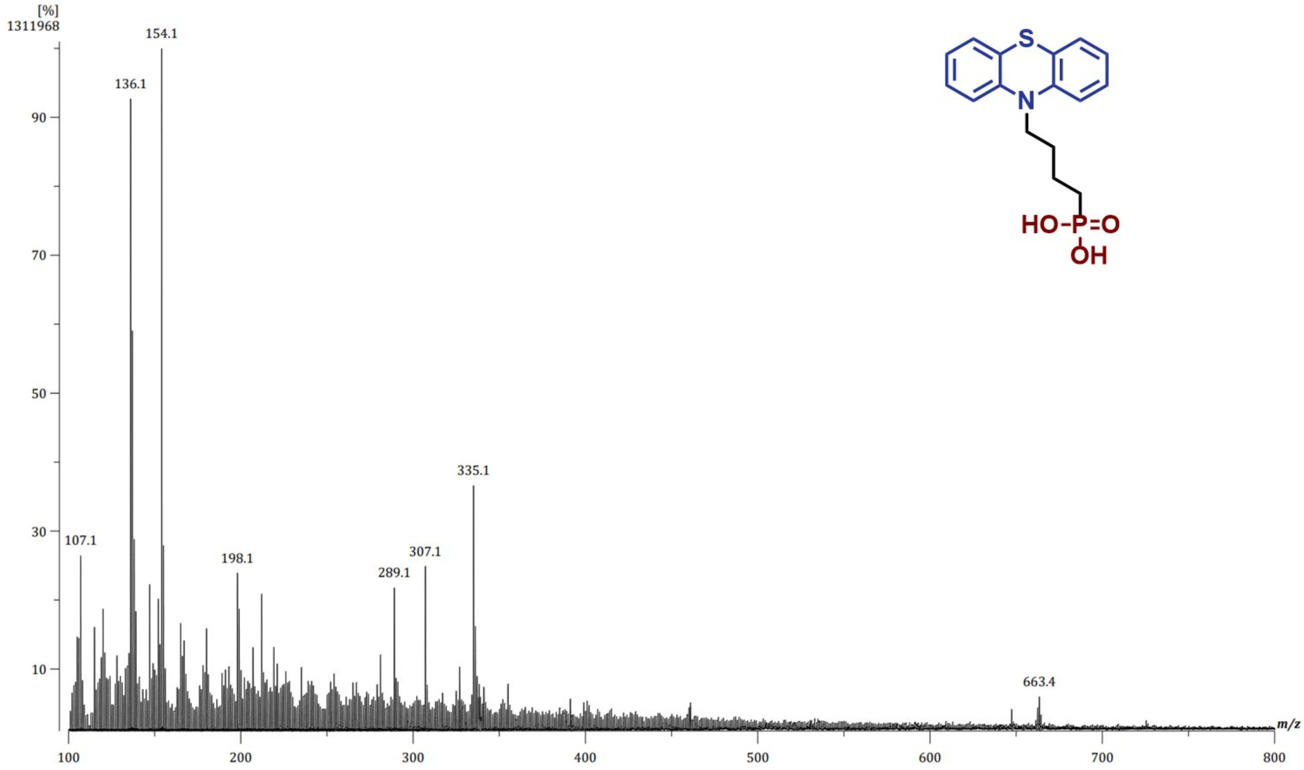

Figure S14. HRMS spectrum of **PTz** (**2**).

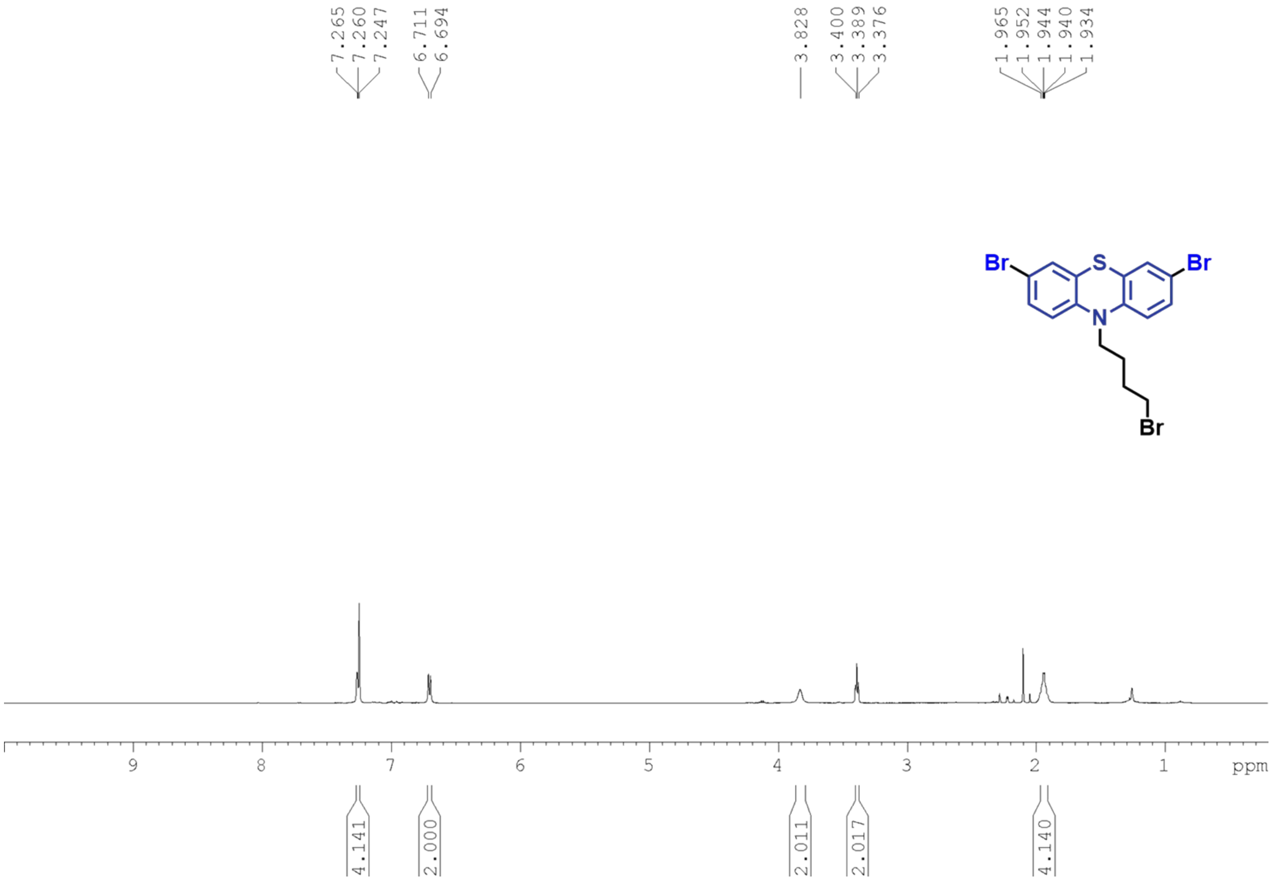

Figure S15. ^{1}H NMR spectrum of compound **8** in $CDCl_3$.

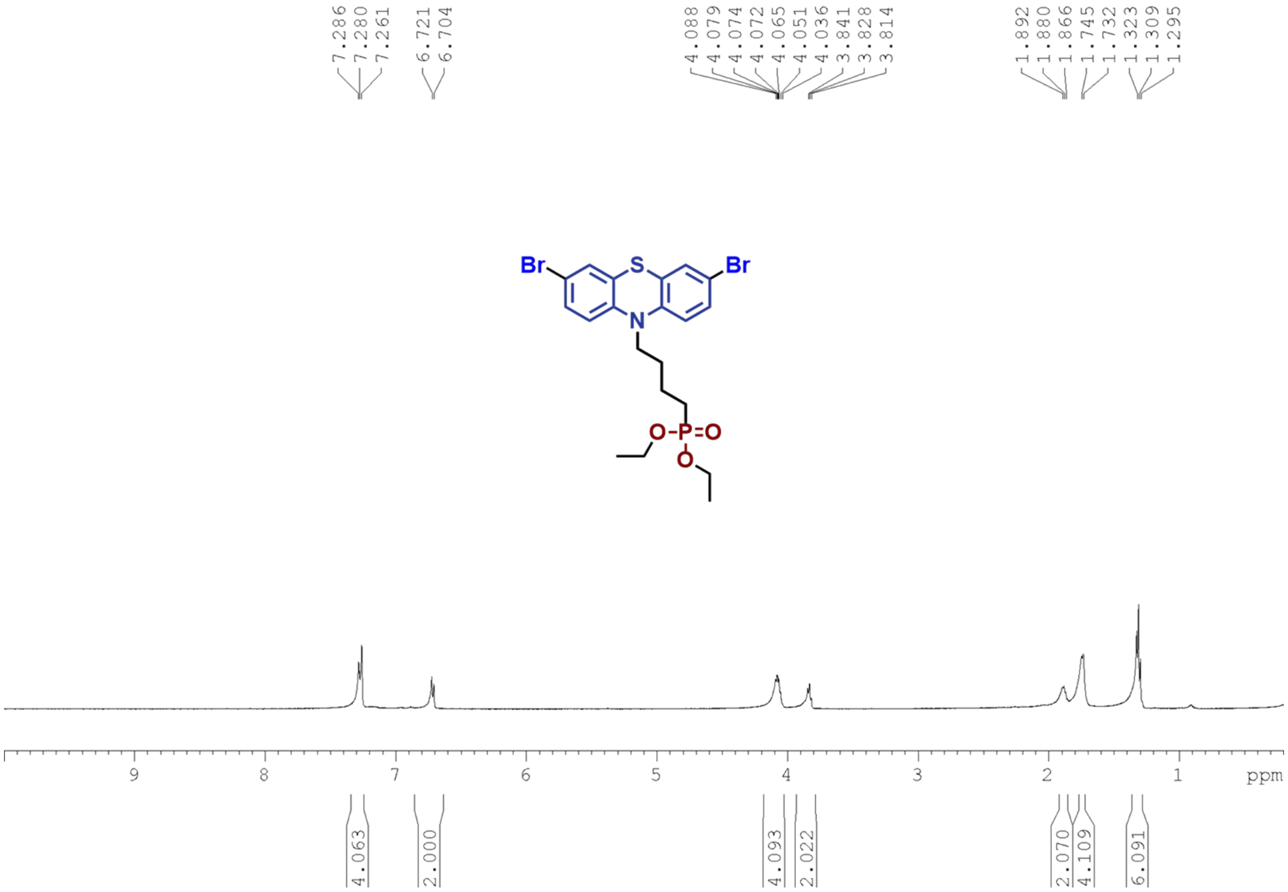

Figure S16. ^{1}H NMR spectrum of compound **9** in $CDCl_3$.

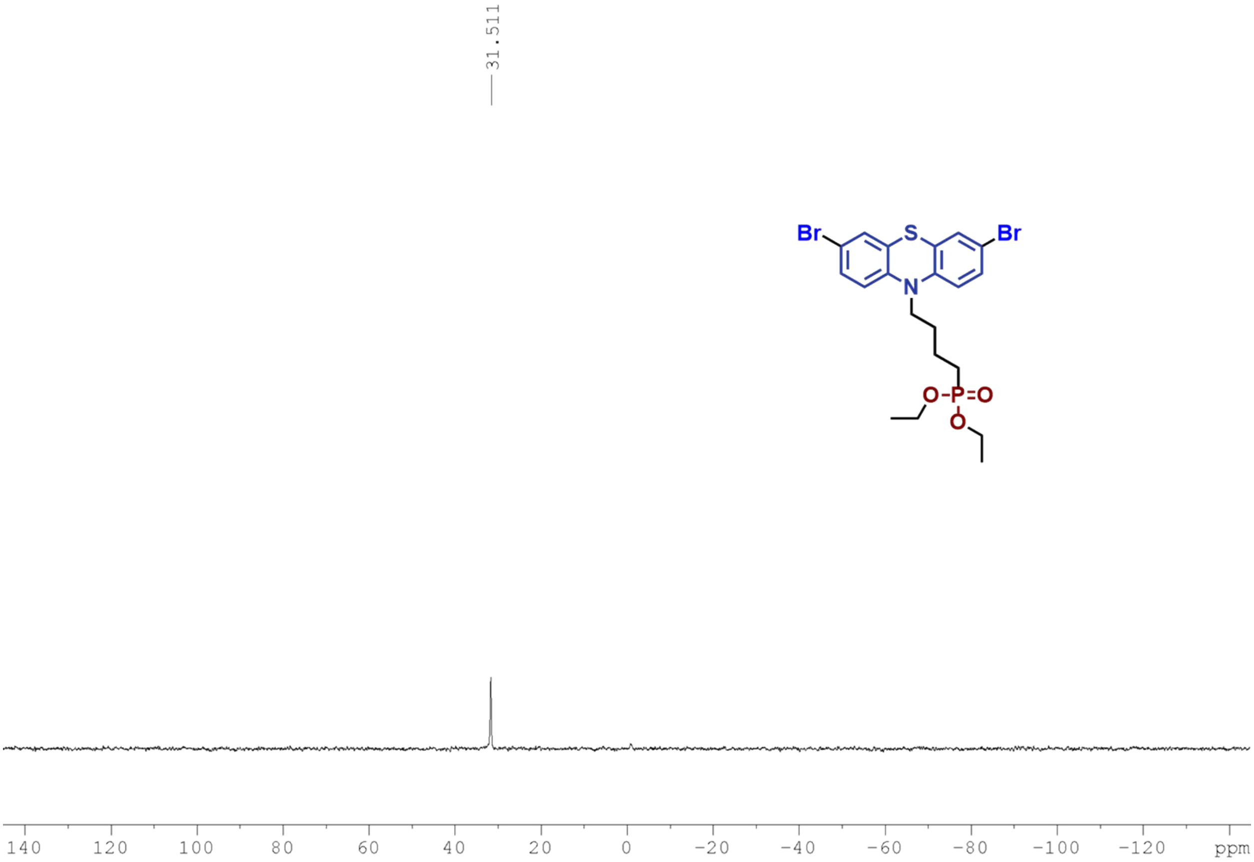

Figure S17. ^{31}P NMR spectrum of compound **9** in $CDCl_3$.

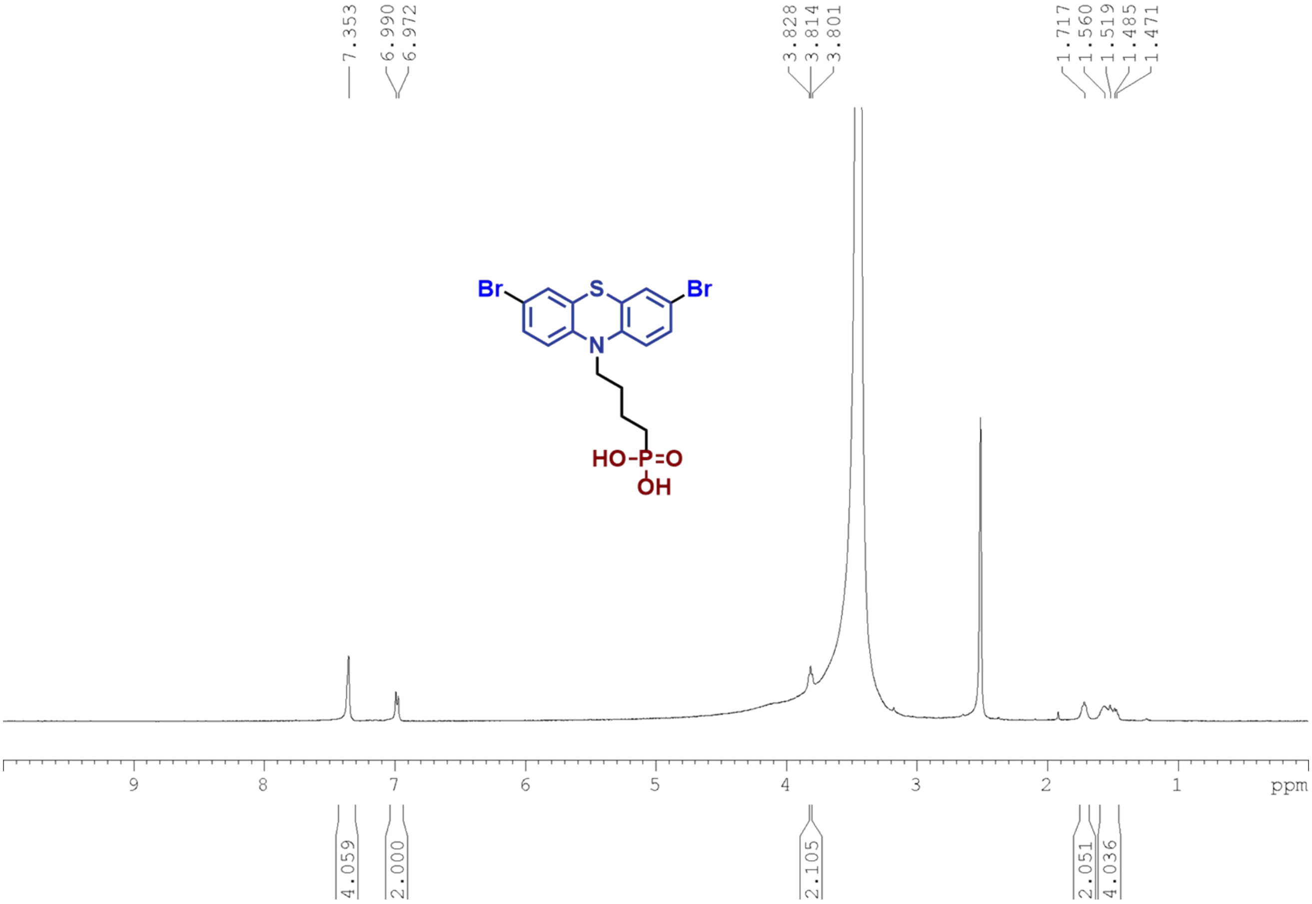

Figure S18. ^{1}H NMR spectrum of **PTzBr** (**3**) in DMSO-d_6.

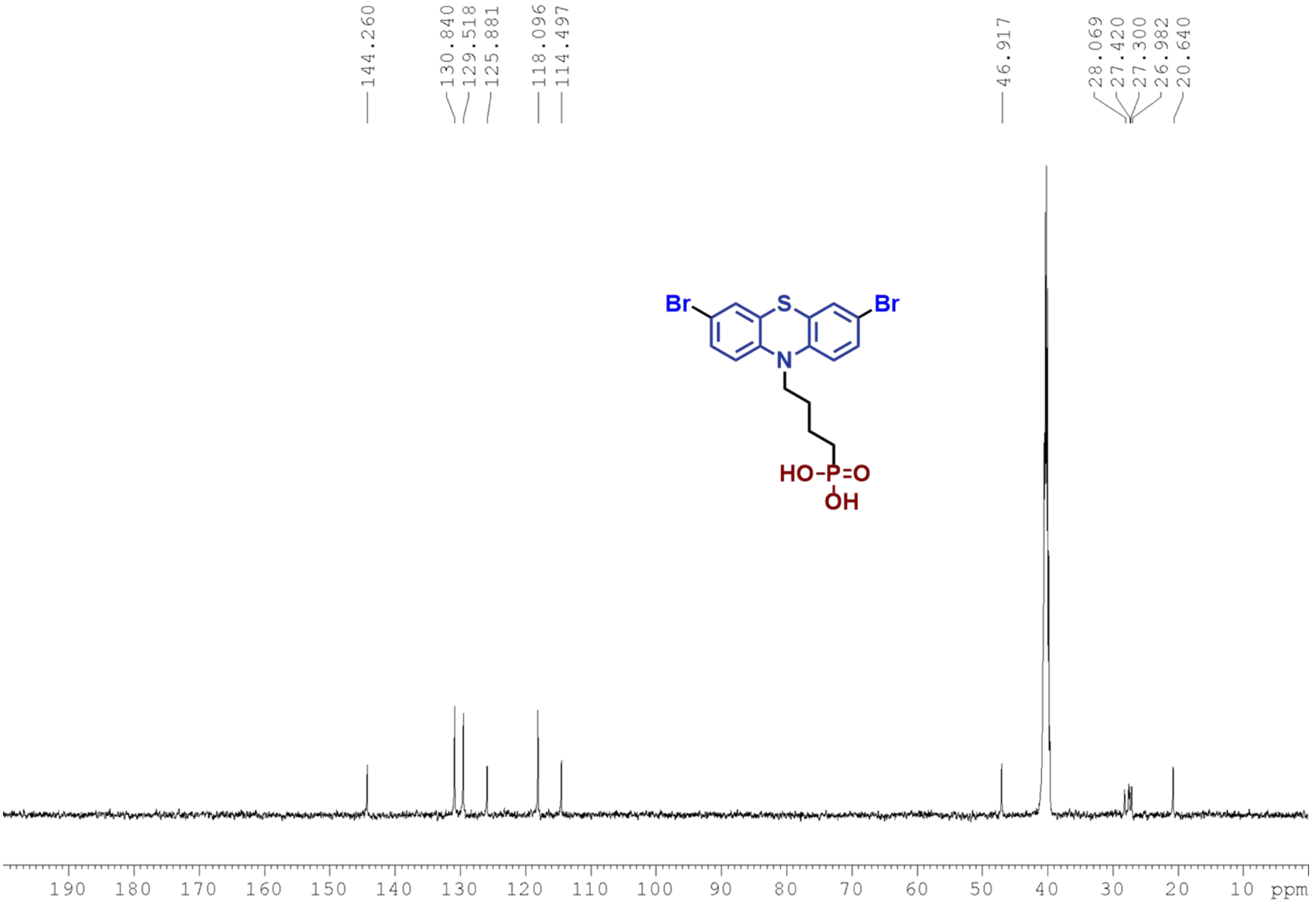

Figure S19. ^{13}C NMR spectrum of **PTzBr** (**3**) in DMSO-d_6.

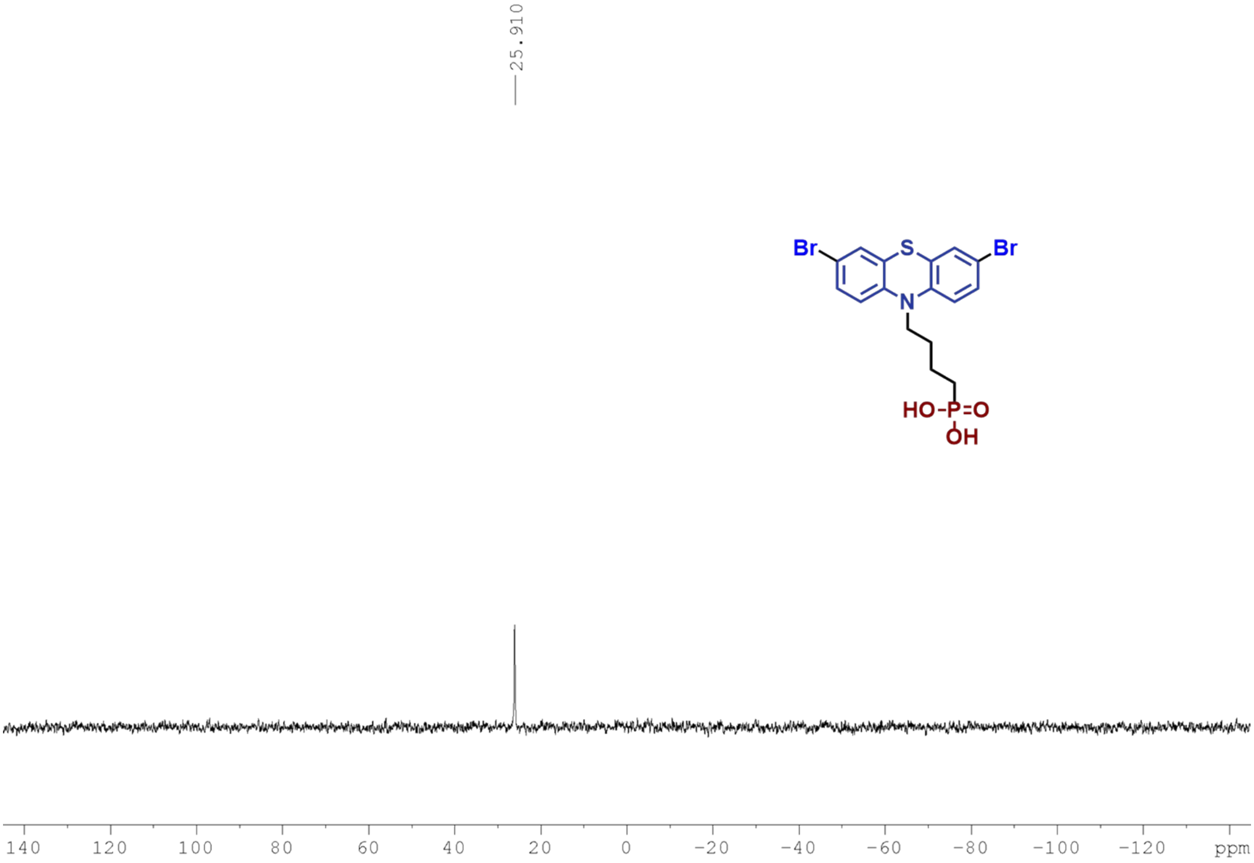

Figure S20. ^{31}P NMR spectrum of **PTzBr** (**3**) in DMSO-d_6.

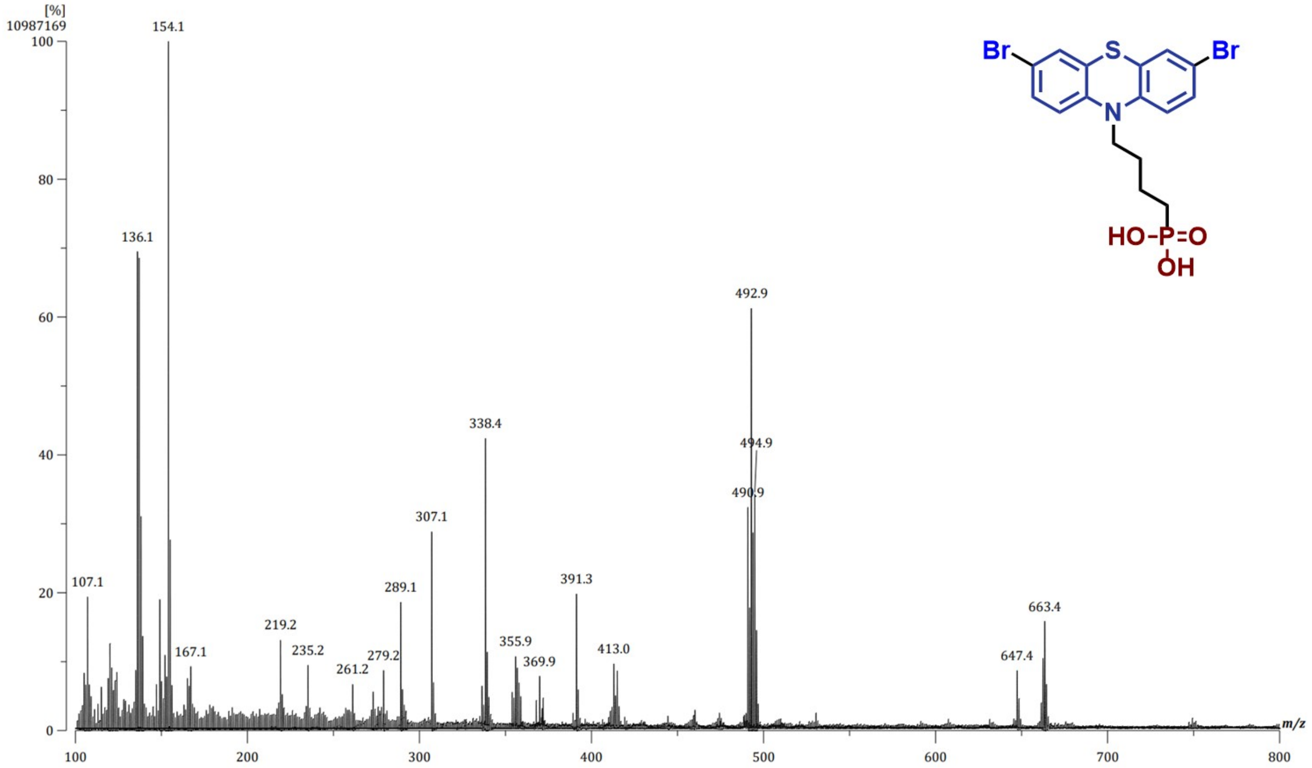

Figure S21. HRMS spectrum of **PTzBr** (**3**).

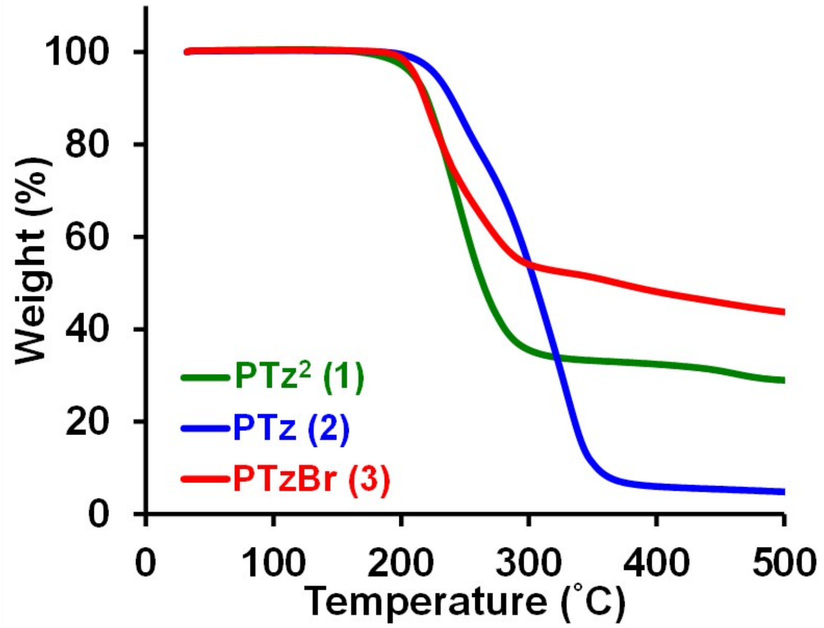

Figure S22. TGA curves of phenothiazine-based SAM molecules **1**-**3**.

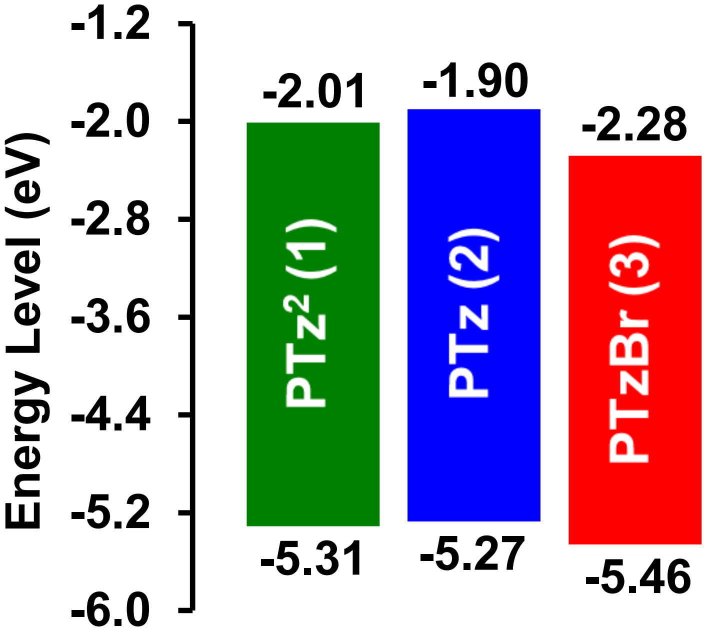

Figure S23. Energy level diagram of phenothiazine-based SAM molecules **1-3** obtained from DPV.

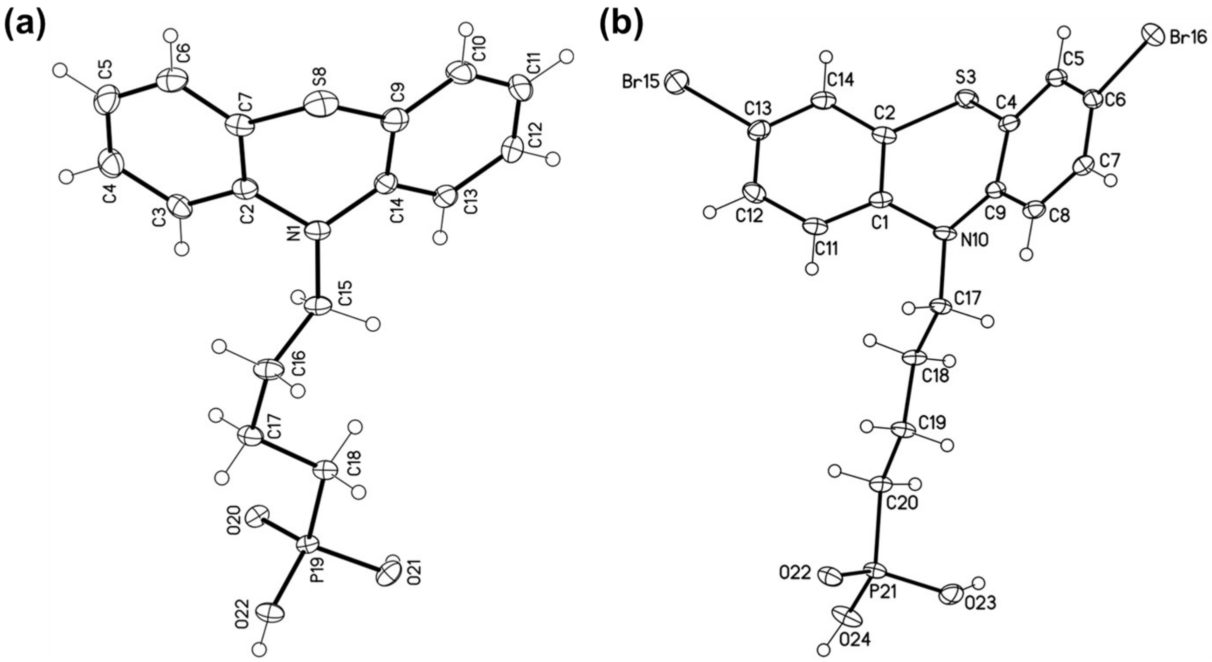

Figure S24. Perspective ORTEP drawing of the molecular structures of **PTz** (**2**) and **PTzBr** (**3**).

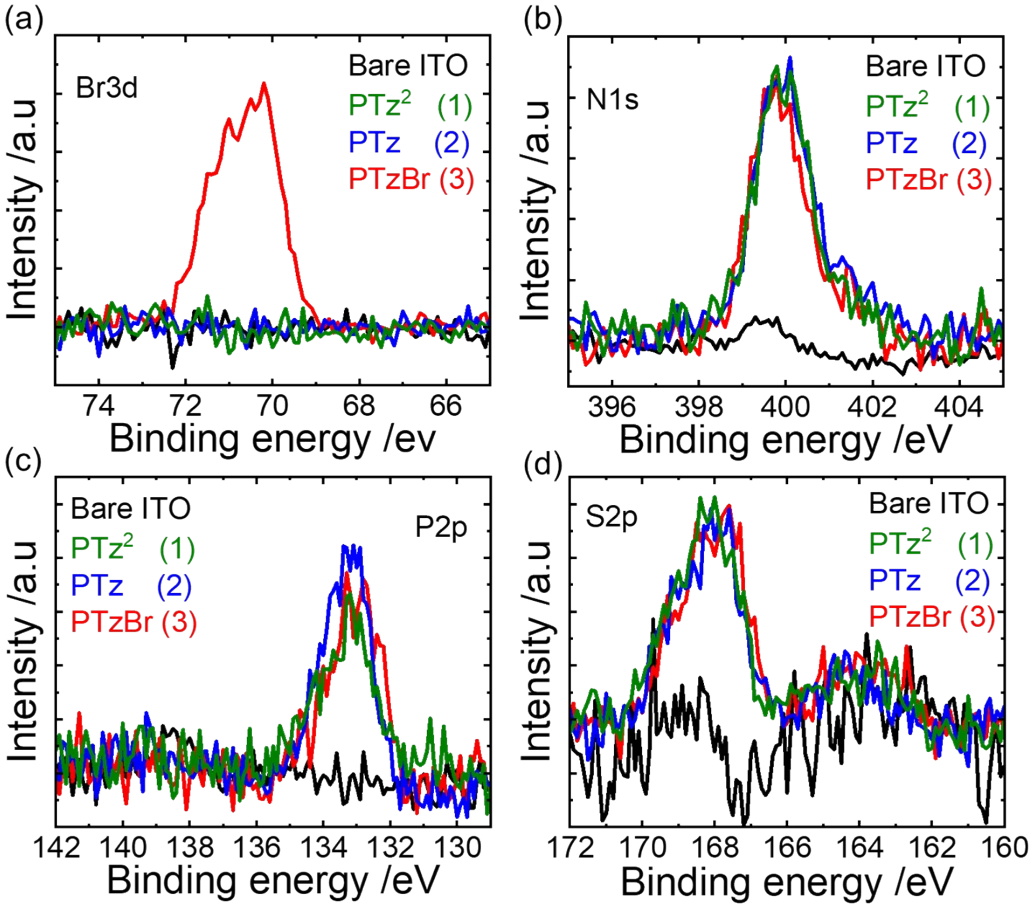

Figure S25. X-ray Photoelectron spectra confirms the successful functionalization of SAM; **PTz^2 (1), PTz (2)**, and **PTzBr (3)** on ITO substrates through the presence of (a) Br3d, (b) N1s, (c) P2p, and (d) S2p region. The XPS spectra of the bare ITO substrate without SAM is also shown here for comparison.

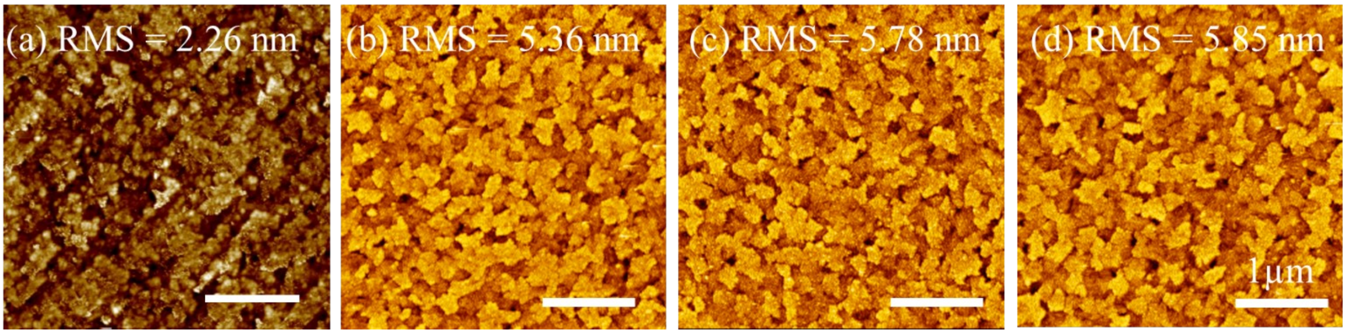

Figure S26. The AFM images of SAM **1-3** with rms values of SAM coated on ITO substrates, (a) Bare ITO (b) **PTzBr (3)**, (c) **PTz (2)**, and (d) **PTz^2 (1)**.

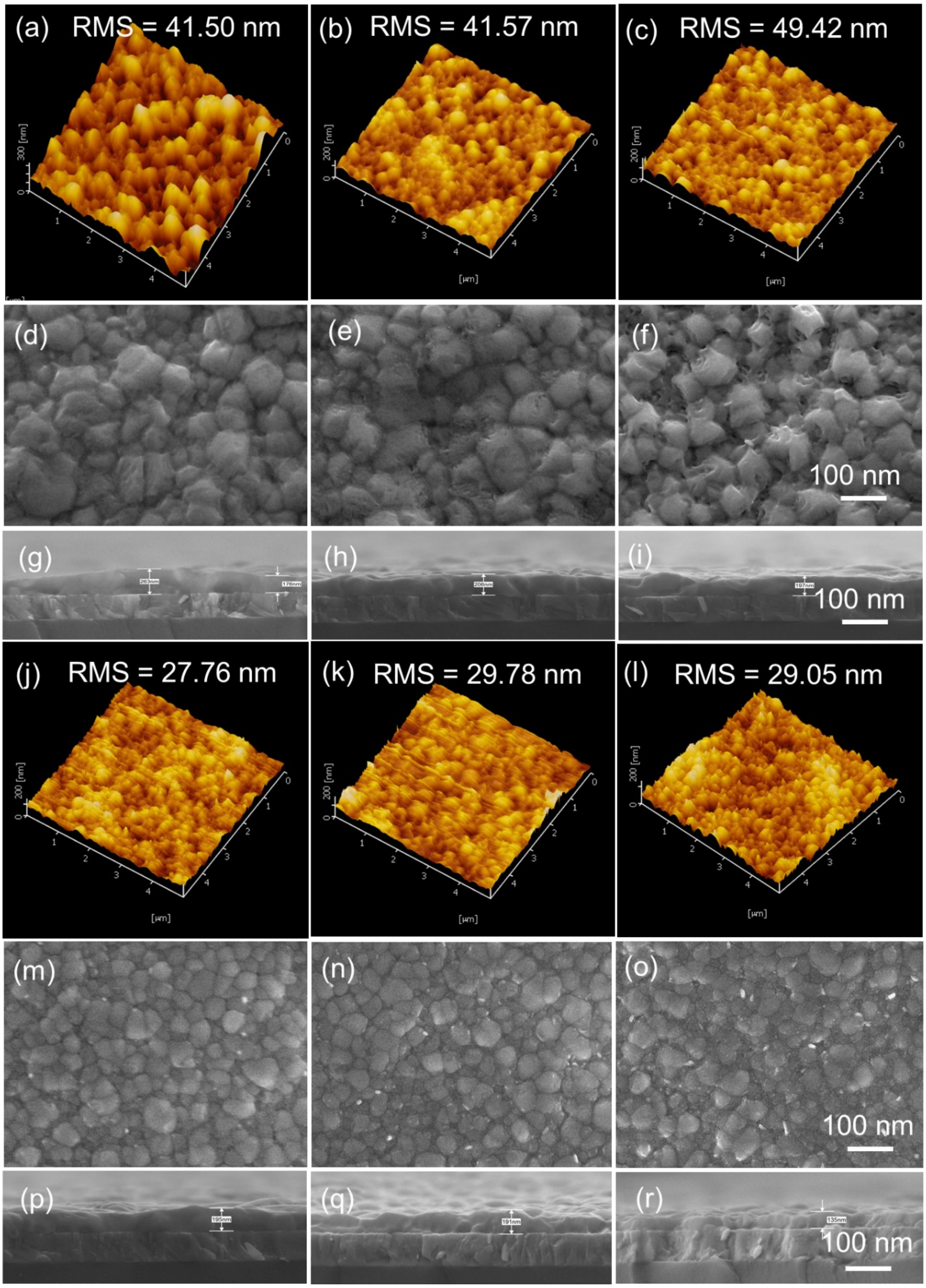

Figure S27. AFM roughness images (a-c), SEM top-view morphologies (d-f), and SEM cross sectional images (g-i) of the $FA_{0.75}MA_{0.25}SnI_3$ based perovskite film and AFM roughness images (j-l), SEM top-view morphologies (m-o), and SEM cross sectional images (p-r) of the $FASnI_3$ based perovskite films prepared over the SAMs, **PTzBr** (**3**), **PTz** (**2**) and **PTz2** (**1**), coated on ITO substrates, respectively.

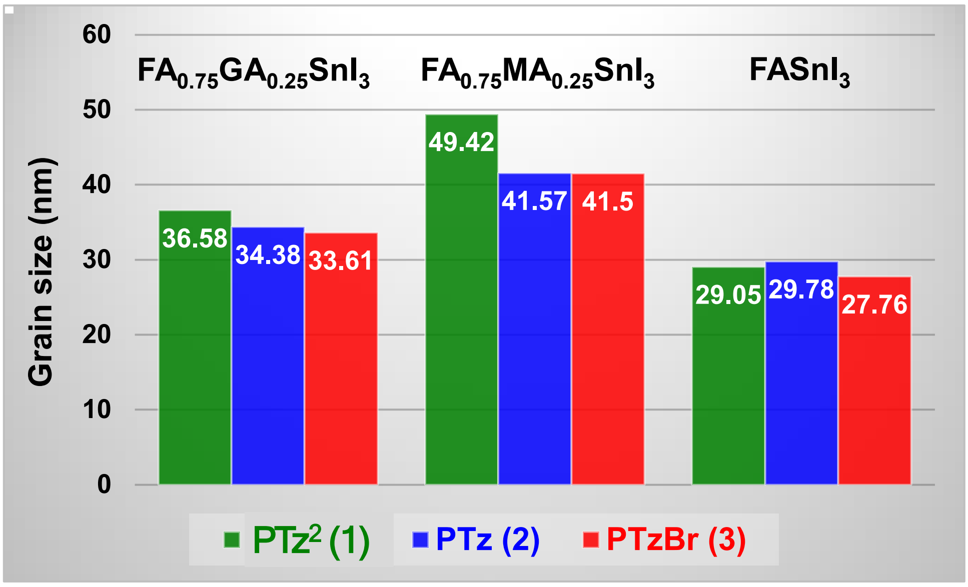

Figure S28. Histographical representation of grain sizes extracted from SEM images of various perovskite films fabricated using three different SAMs, showing the distribution and variation of grain sizes for each composition.

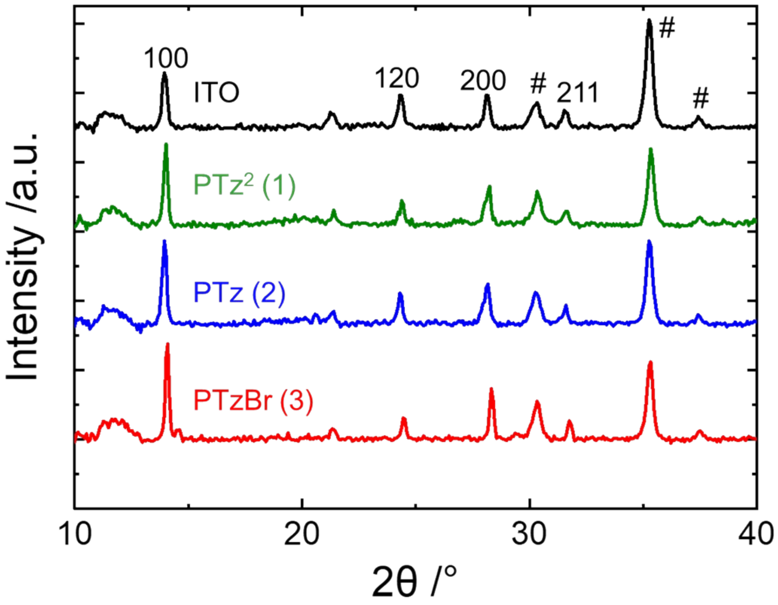

Figure S29. The XRD patterns of the SAM/PSK samples, with the exposed planes of the $FA_{0.75}GA_{0.25}SnI_3$-based perovskite crystal indicated, alongside those of ITO denoted by #, were recorded.

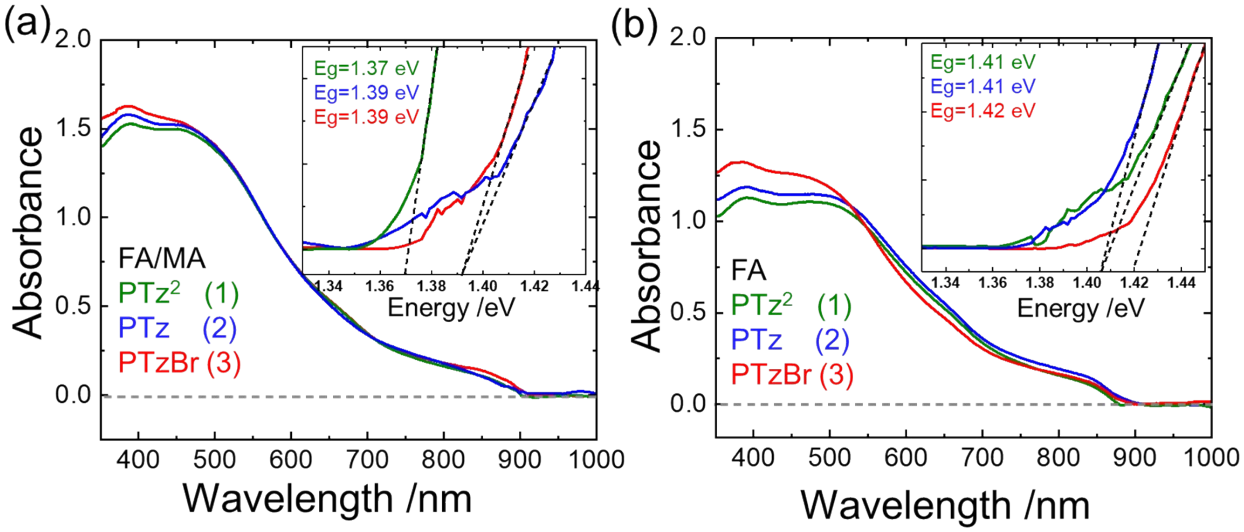

Figure S30. UV-visible absorption spectra of (a) $FA_{0.75}MA_{0.25}SnI_3$ and (b) $FASnI_3$ based perovskite films formed on SAM**; PTz^2** (**1**), **PTz** (**2**), and **PTzBr** (**3**), on ITO substrates, respectively.

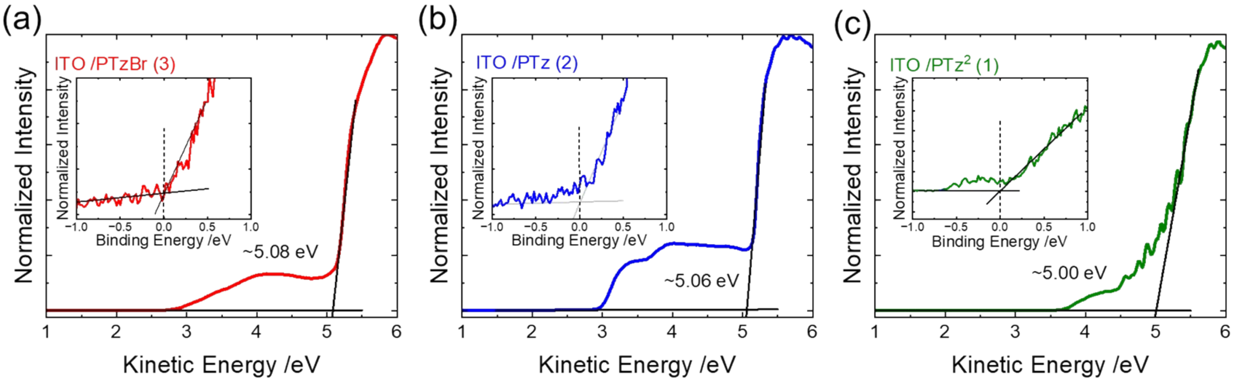

Figure S31. The UPS spectra illustrate the low kinetic energy regions of SAMs (a) **PTzBr** (**3**), (b) **PTz** (**2**), and (c) **PTz^2** (**1**) coated on ITO substrates. The work functions were estimated from the linear fits, as shown. The insets depict the onset of the spectra near the low binding energy region, around 0 eV for all three SAMs.

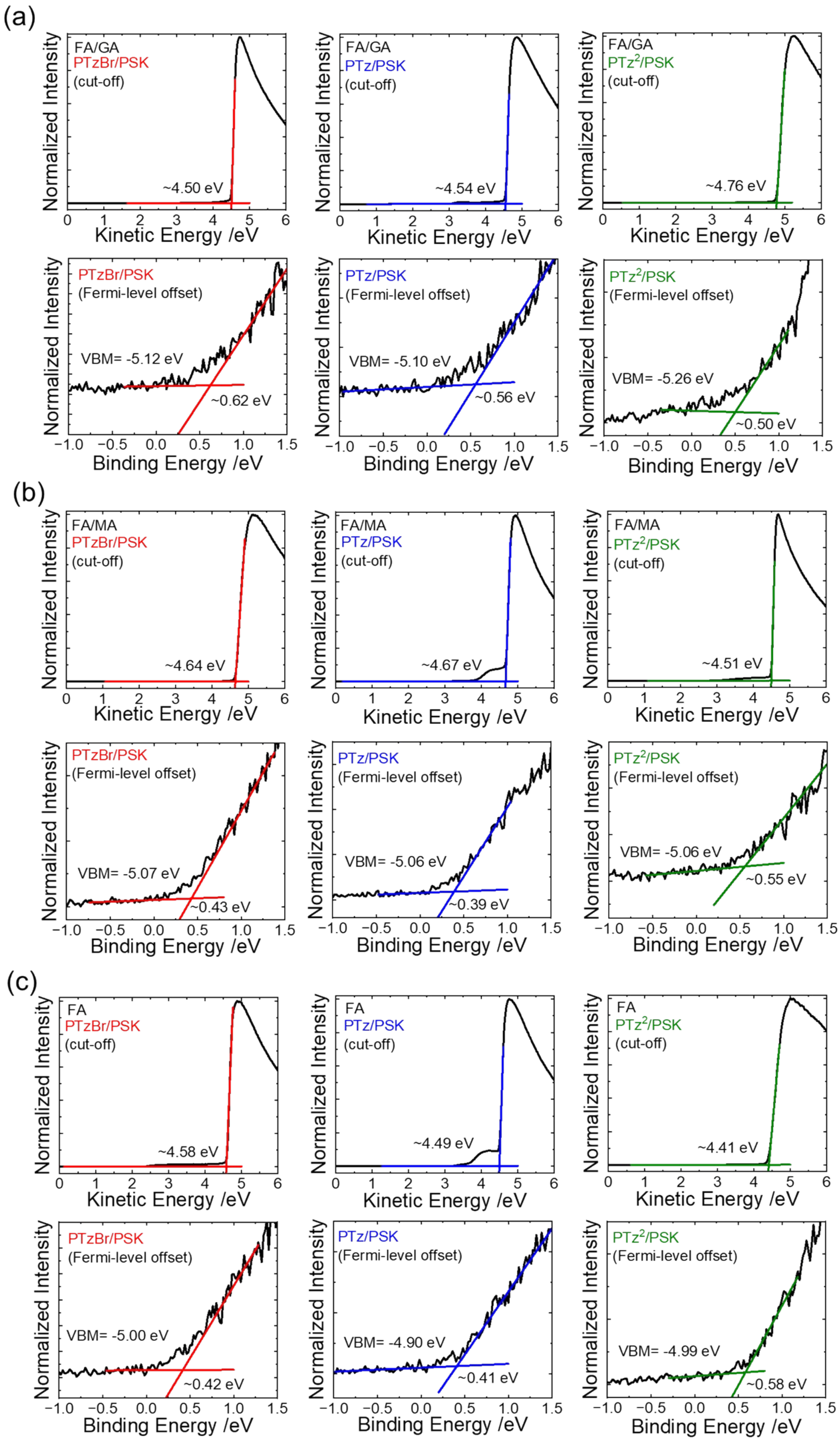

Figure S32. Fermi-level offset (low binding energy region), and secondary electron cut-off (low kinetic energy region) of the perovskite films on **PTzBr** (**3**), **PTz** (**2**), and **PTz²** (**1**) from UPS spectra corresponding to (a) $FA_{0.75}GA_{0.25}SnI_3$, (b) $FA_{0.75}MA_{0.25}SnI_3$, and (c) $FASnI_3$, respectively.

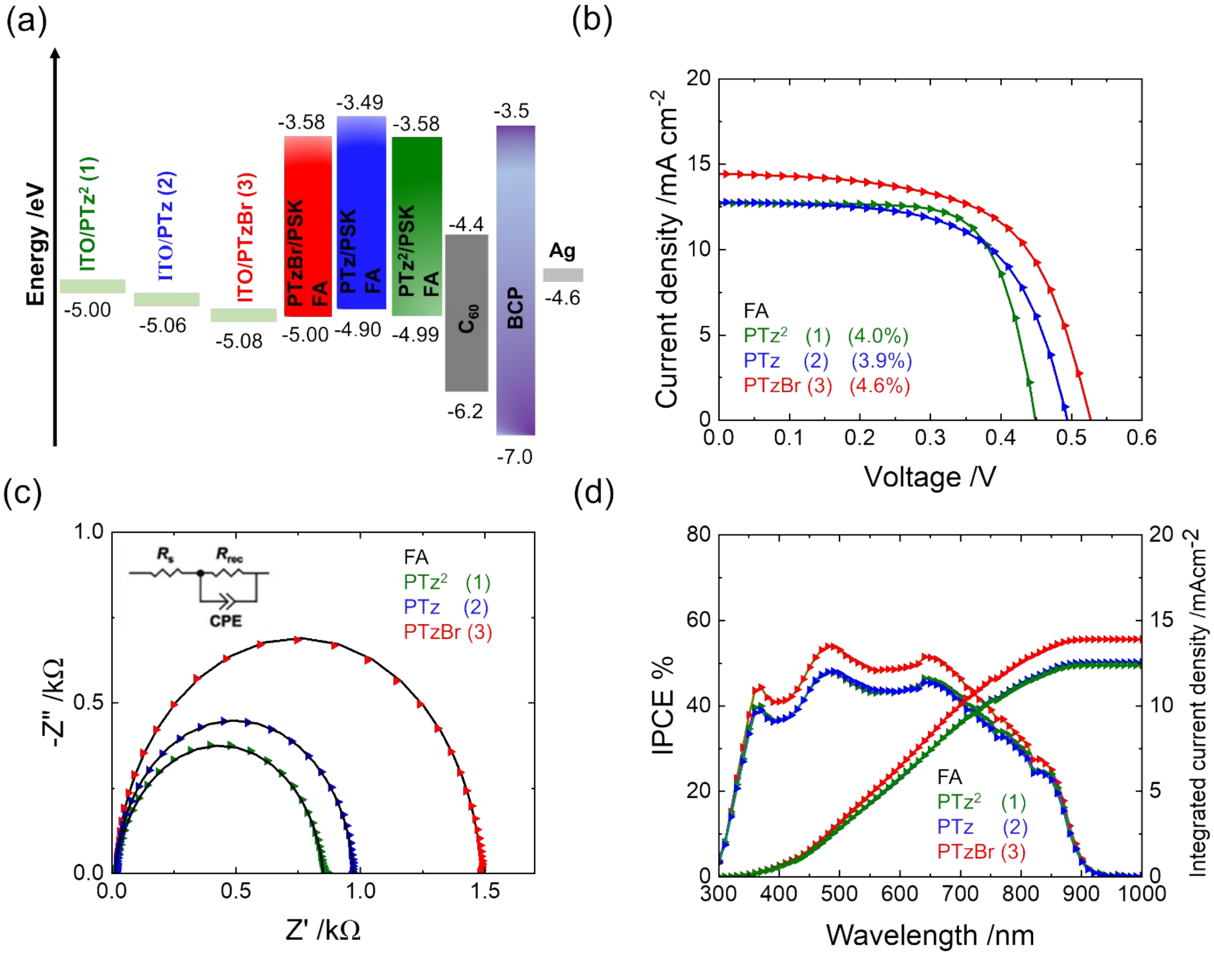

Figure S33. (a) Energy-level diagram, (b) J-V characteristics, (c) EIS Nyquist plots, and (d) IPCE spectra, for the devices of **PTz^2 (1), PTz (2),** and **PTzBr (3)** made of FASnI$_3$ perovskite precursor.

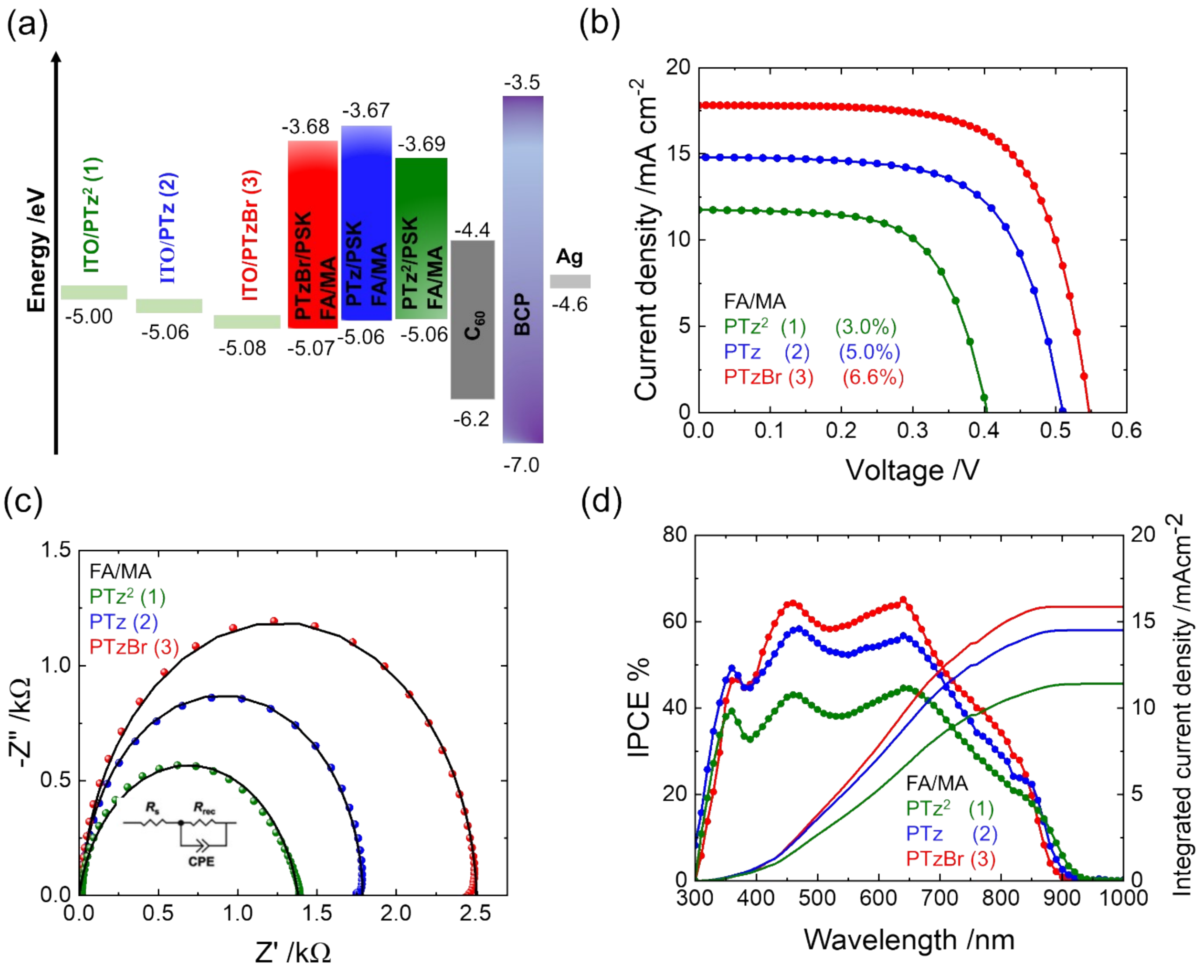

Figure S34. (a) Energy-level diagram, (b) J-V characteristics, (c) EIS Nyquist plots, and (d) IPCE spectra, for the devices of **PTz² (1), PTz (2)**, and **PTzBr (3)** made of $FA_{0.75}MA_{0.25}SnI_3$ perovskite precursor.

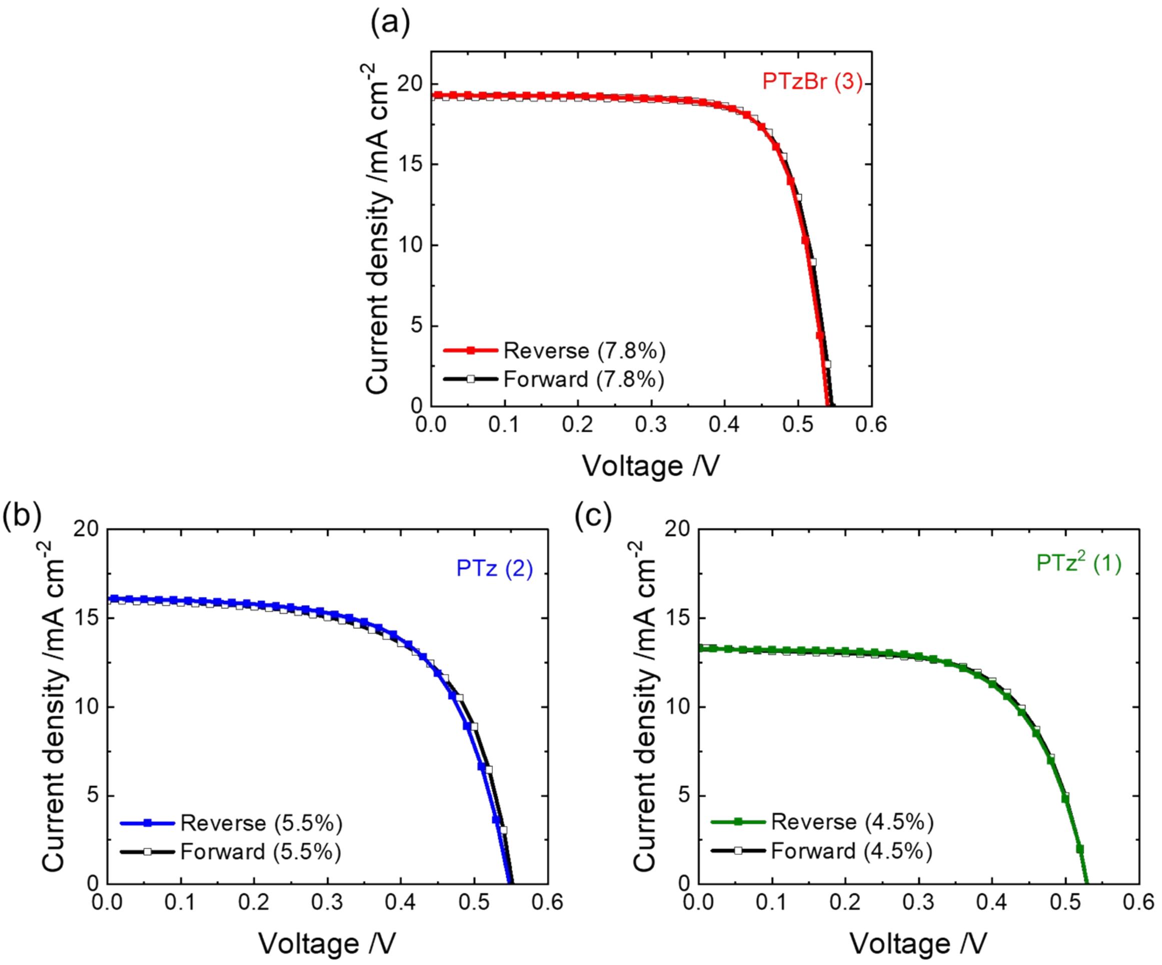

Figure S35. Forward and reverse scans of the *J*-*V* curves of the champion (a) **PTzBr (3),** (b) **PTz (2)**, and (c) **PTz^2 (1)** SAM based devices showing the negligible effect of hysteresis.

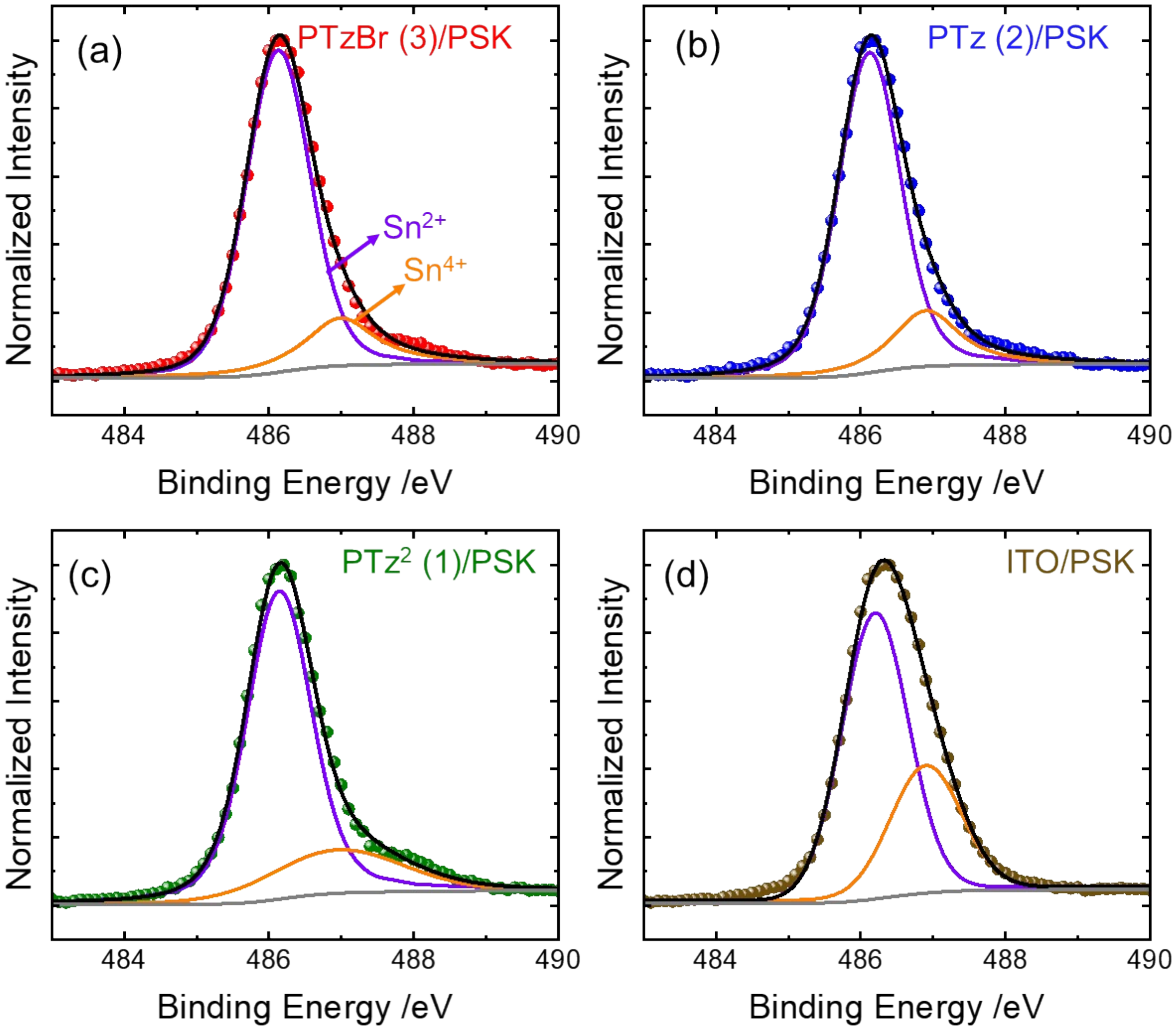

Figure S36. Sn 3d XPS spectra obtained from the surface of perovskite samples with SAMs as shown, **(a) PTzBr (3)/PSK, (b) PTz (2)/PSK**, **(c) PTz^2 (1)/PSK, (d) ITO/PSK**

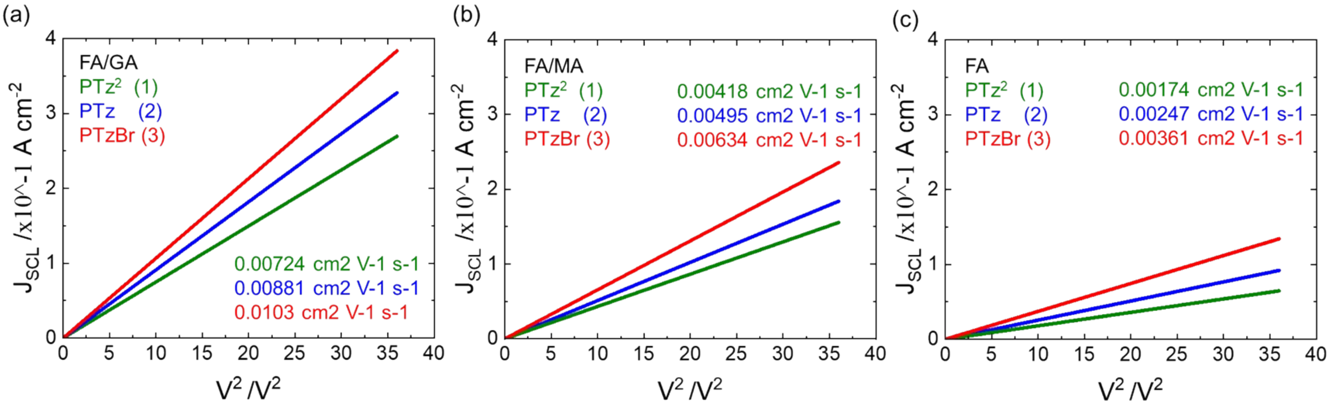

Figure S37. SCLC measurements with SAMs **PTzBr** (**3**), **PTz** (**2**), and **PTz²** (**1**) as indicated, made of (a) $FA_{0.75}GA_{0.25}SnI_3$, (b) $FA_{0.75}MA_{0.25}SnI_3$, (c) FA based perovskite precursor.

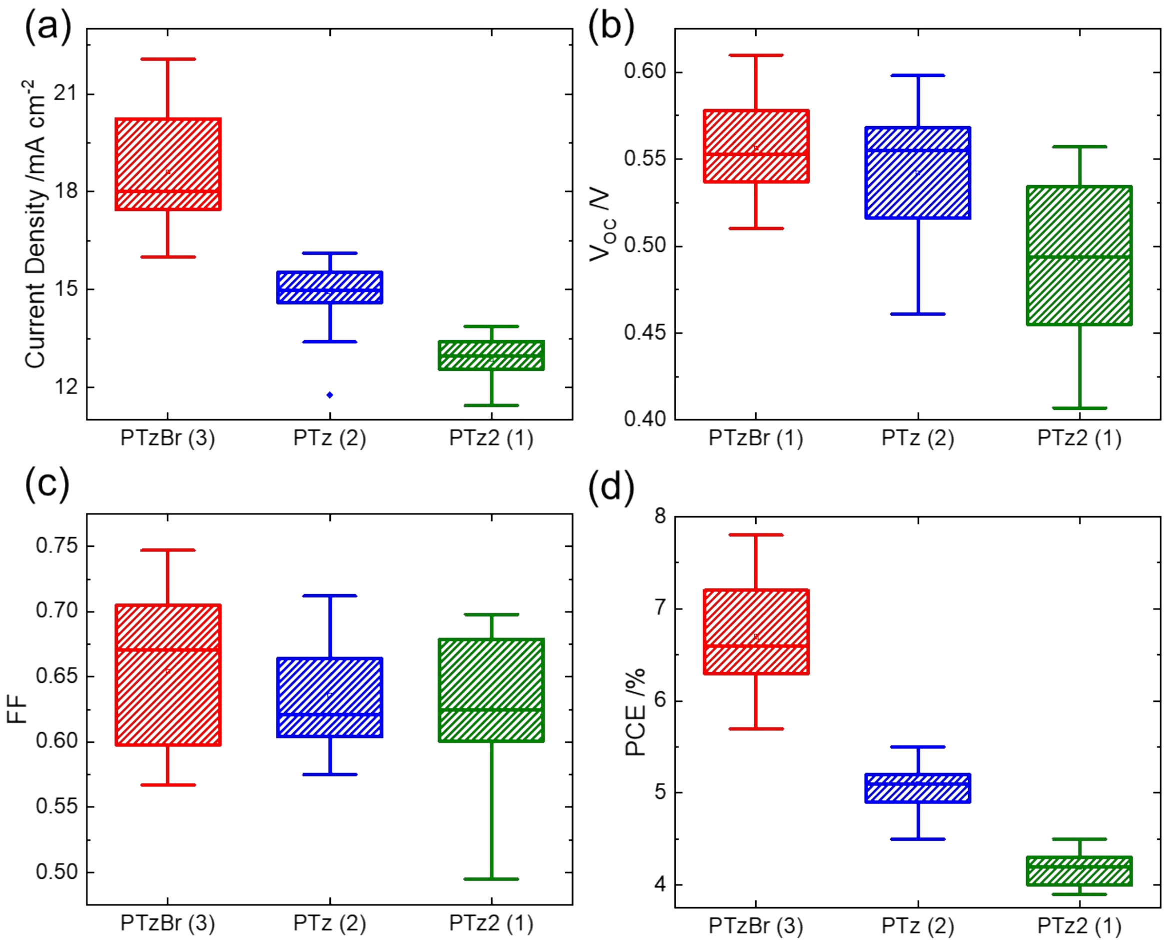

Figure S38. Statistical analysis performed on 25 devices of $FA_{0.75}GA_{0.25}SnI_3$ fabricated with on **PTzBr (3), PTz (2),** and **PTz² (1)** SAMs coated on ITO substrates. Data for (a) J_{SC}, (b) V_{OC}, (c) FF, and (d) PCE are reported.

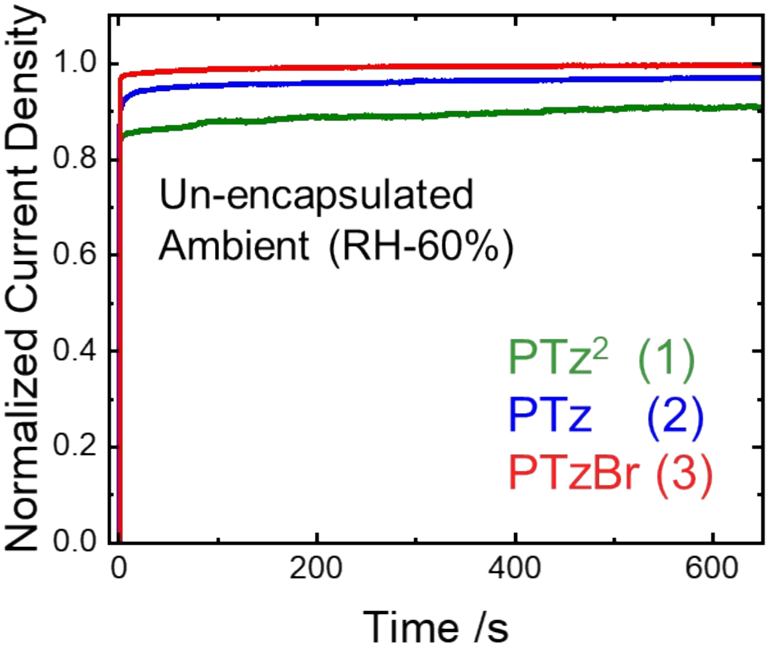

Figure S39. Maximum power point (MPP) tracking of $FA_{0.75}GA_{0.25}SnI_3$-based perovskite devices, deposited on SAMs, including **PTz²** (**1**), **PTz** (**2**), and **PTzBr** (**3**), during a 600 second light-soaking test without encapsulation under ambient conditions.

Table S1. Summary of crystal structure data for **PTz** (**2**).

Identification code	240916lt_auto
Empirical formula	$C_{16}H_{18}NO_3PS$
Formula weight	335.34
Temperature/K	100.00(10)
Crystal system	orthorhombic
Space group	Iba2
a/Å	29.9399(3)
b/Å	13.61034(13)
c/Å	7.71770(7)
α/°	90
β/°	90
γ/°	90
Volume/Å^3	3144.90(5)
Z	8
ρ_{calc}g/cm^3	1.417
μ/mm^{-1}	2.896
F(000)	1408.0
Crystal size/mm^3	0.32 × 0.06 × 0.04
Radiation	Cu Kα (λ = 1.54184)
2Θ range for data collection/°	7.134 to 134.152
Index ranges	$-35 \leq h \leq 35$, $-16 \leq k \leq 16$, $-9 \leq l \leq 6$
Reflections collected	20064
Independent reflections	2368 [R_{int} = 0.0278, R_{sigma} = 0.0152]
Data/restraints/parameters	2368/1/202
Goodness-of-fit on F^2	1.048
Final R indexes [I>=2σ (I)]	R_1 = 0.0246, wR_2 = 0.0657
Final R indexes [all data]	R_1 = 0.0249, wR_2 = 0.0660
Largest diff. peak/hole / e Å^{-3}	0.19/-0.21
Flack parameter	-0.027(18)

Crystallographic data (excluding structure factors) for the structure(s) reported in this paper have been deposited with the Cambridge Crystallographic Data Centre as supplementary publication no. **CCDC 2383214**.

Table S2. Summary of crystal structure data for **PTzBr** (**3**).

Identification code	241020LT_auto
Empirical formula	$C_{16}H_{16}Br_2NO_3PS$
Formula weight	493.15
Temperature/K	99.99(10)
Crystal system	monoclinic
Space group	C2/c
a/Å	38.4715(5)
b/Å	8.07574(11)
c/Å	11.33025(15)
α/°	90
β/°	91.3729(12)
γ/°	90
Volume/Å^3	3519.13(8)
Z	8
ρ_{calc}g/cm^3	1.862
μ/mm^{-1}	7.953
F(000)	1952.0
Crystal size/mm^3	0.08 × 0.06 × 0.02
Radiation	Cu Kα (λ = 1.54184)
2Θ range for data collection/°	9.198 to 145.686
Index ranges	$-46 \leq h \leq 47$, $-9 \leq k \leq 9$, $-12 \leq l \leq 13$
Reflections collected	10590
Independent reflections	3386 [R_{int} = 0.0226, R_{sigma} = 0.0228]
Data/restraints/parameters	3386/0/220
Goodness-of-fit on F^2	1.035
Final R indexes [I>=2σ (I)]	R_1 = 0.0237, wR_2 = 0.0604
Final R indexes [all data]	R_1 = 0.0259, wR_2 = 0.0615
Largest diff. peak/hole / e Å^{-3}	0.48/-0.69

Crystallographic data (excluding structure factors) for the structure(s) reported in this paper have been deposited with the Cambridge Crystallographic Data Centre as supplementary publication no. **CCDC 2389332**.

Table S3. Curve fitting results of the TCSPC decay in **Figure 5d**.

Sample	**$\tau_1(\alpha_1)$ /ns**	**$\tau_2(\alpha_2)$ /ns**	**τ_{avg} /ns**
PTzBr (3)/PSK (FA/GA)	4.89 (0.11)	1.57 (0.89)	2.5
PTz (2)/PSK (FA/GA)	4.99 (0.2)	1.94 (0.8)	3.1
PTz^2 (1)/PSK (FA/GA)	6.99 (0.19)	2.72 (0.81)	4.3

The average PL lifetimes (τ_{avg}) were calculated by using the intensity average method, given by $\tau_{avg} = (\alpha_1\tau_1^2 + \alpha_2\tau_2^2)/(\alpha_1\tau_1 + \alpha_2\tau_2)$

Table S4. Proportions of Sn^{2+} and Sn^{4+} in the perovskite samples, as determined from the XPS spectra shown in **Figure S34.**

Sample	**Sn^{2+}**	**Sn^{4+}**
PTzBr (3)/PSK	82.7%	17.3%
PTz (2)/PSK	81.8%	18.2%
PTz^2 (1)/PSK	80.2%	19.8%
ITO/PSK	68.7%	31.3%

Table S5. Photovoltaic parameters of best-performing $FASnI_3$ based devices corresponding to statistic of *J-V* curves in **Figure S31b.**

Device	V_{OC} /V	J_{SC} /mA cm^{-2}	Integrated J_{SC}	FF /%	PCE /%
PTzBr (3)	0.530	14.45	13.93	0.605	4.6
PTz (2)	0.452	12.75	12.22	0.681	3.9
PTz^2 (1)	0.447	12.75	12.75	0.704	4.0

Table S6. Photovoltaic parameters of best-performing $FA_{0.75}MA_{0.25}SnI_3$ based devices corresponding to statistic of *J-V* curves in **Figure S32b.**

Device	V_{OC} /V	J_{SC} /mA cm^{-2}	Integrated J_{SC}	FF /%	PCE /%
PTzBr (3)	0.548	17.79	16.14	0.677	6.6
PTz (2)	0.511	14.86	14.73	0.649	5.0
PTz^2 (1)	0.406	11.75	11.57	0.636	3.0

Table S7. Photovoltaic cell parameters of **PTzBr (3)** devices as obtained from the data shown in **Fig. S36.**

Device No.	*Jsc* /mA cm^{-2}	*Voc* /V	FF	PCE /%
1	18.00	0.571	0.702	7.2
2	20.31	0.578	0.606	7.1
3	21.08	0.578	0.587	7.1
4	17.96	0.574	0.594	6.1
5	18.07	0.575	0.612	6.3
6	17.67	0.552	0.671	6.5
7	17.79	0.548	0.677	6.6
8	19.19	0.548	0.747	7.8

9	16.89	0.605	0.567	5.8
10	18.50	0.537	0.705	7.0
11	18.38	0.536	0.703	6.9
12	21.53	0.554	0.613	7.3
13	17.76	0.585	0.625	6.5
14	16.96	0.589	0.632	6.3
15	17.45	0.610	0.589	6.2
16	21.31	0.581	0.573	7.1
17	22.06	0.553	0.598	7.3
18	16.99	0.520	0.650	5.7
19	16.18	0.539	0.717	6.2
20	15.99	0.529	0.724	6.1
21	16.54	0.541	0.712	6.3
22	17.59	0.510	0.707	6.3
23	20.24	0.523	0.688	7.3
24	21.75	0.553	0.598	7.2
25	19.05	0.521	0.724	7.2
Mean ± s.d.	18.17 ± 2.22	0.575± 0.01	0.656 ± 0.04	7.0 ± 0.32

Table S8. Photovoltaic cell parameters of **PTz (2)** devices as obtained from the data shown in **Fig. S36.**

Device No.	***Jsc*** **/mA cm^{-2}**	***Voc*** **/V**	**FF**	**PCE** **/%**
1	15.96	0.558	0.604	5.4
2	15.32	0.532	0.628	5.1
3	14.43	0.585	0.612	5.1
4	14.63	0.588	0.593	5.1
5	15.73	0.461	0.710	5.1
6	15.75	0.464	0.712	5.2
7	16.00	0.558	0.617	5.5
8	15.93	0.563	0.575	5.1
9	11.77	0.598	0.697	4.9
10	14.99	0.589	0.589	5.2
11	14.95	0.590	0.582	5.1
12	14.60	0.576	0.620	5.2
13	15.46	0.522	0.645	5.2
14	15.43	0.530	0.650	5.3
15	14.46	0.555	0.613	4.9
16	14.21	0.563	0.601	4.8
17	13.39	0.568	0.590	4.5
18	13.46	0.525	0.670	4.7
19	14.86	0.469	0.707	4.9
20	14.88	0.516	0.656	5.0
21	14.86	0.511	0.649	4.9
22	15.48	0.555	0.610	5.2
23	15.24	0.505	0.664	5.1
24	15.53	0.516	0.691	5.5
25	16.11	0.554	0.621	5.5
Mean ± s.d.	15.55 ± 0.716	0.565 ± 0.02	0.620 ± 0.01	5.1 ± 0.2

Table S9. Photovoltaic cell parameters of **PTz^2 (1)** devices as obtained from the data shown in **Fig. S36.**

Device No.	***Jsc*** **/mA cm^{-2}**	***Voc*** **/V**	**FF**	**PCE** **/%**
1	11.54	0.514	0.679	4.0
2	12.57	0.537	0.625	4.2
3	13.87	0.507	0.601	4.2
4	12.60	0.543	0.620	4.2
5	11.62	0.556	0.651	4.2
6	13.20	0.535	0.646	4.5
7	13.26	0.556	0.585	4.3
8	13.20	0.494	0.689	4.5
9	12.80	0.493	0.698	4.4
10	13.68	0.442	0.697	4.2
11	13.41	0.511	0.605	4.1
12	12.20	0.535	0.620	4.0
13	12.00	0.544	0.620	4.0
14	13.73	0.410	0.695	3.9
15	12.68	0.407	0.680	4.3
16	11.44	0.412	0.691	3.2
17	12.35	0.482	0.547	3.2
18	13.41	0.529	0.644	4.5
19	13.44	0.531	0.498	3.5
20	13.27	0.534	0.635	4.5
21	13.75	0.554	0.495	3.7
22	12.94	0.517	0.601	4.0
23	12.57	0.528	0.644	4.2
24	12.98	0.555	0.584	4.2
25	13.00	0.545	0.579	4.1
Mean ± s.d.	13.25 ± 0.85	0.540 ± 0.01	0.607 ± 0.05	4.10 ± 0.05

Table S10. Series and recombination resistance of the best-performing devices made of TPSC obtained from the impedance spectra in **Figure 6d, Figure S31c,** and **Figure S32c.**

Device	**Series Resistance (Ω)**	**Recombination Resistance (kΩ)**
PTzBr (3) (FA/GA)	12.82	4.28
PTz (2) (FA/GA)	39.03	1.53
PTz^2(1) (FA/GA)	16.31	1.21
PTzBr (3) (FA/MA)	13.81	1.25
PTz (2) (FA/MA)	14.54	0.93
PTz^2(1) (FA/MA)	18.42	0.50
PTzBr(3) (FA)	17.63	0.75
PTz (2) (FA)	16.04	0.69
PTz^2(1) (FA)	16.52	0.44